Cryo-EM structure of the active, Gs-protein complexed, human CGRP receptor

Yi-Lynn Liang[1]*, Maryam Khoshouei[2*†], Giuseppe Deganutti[3], Alisa Glukhova[1], Cassandra Koole[1], Thomas S. Peat[4], Mazdak Radjainia[1,5], Jürgen M. Plitzko[2], Wolfgang Baumeister[2], Laurence J. Miller[1,6], Deborah L. Hay[7], Arthur Christopoulos[1], Christopher A Reynolds[3], Denise Wootten[1,8¶], Patrick M. Sexton[1,8¶]

1. Drug Discovery Biology and Department of Pharmacology, Monash Institute of Pharmaceutical Sciences, Monash University, Parkville 3052, Victoria, Australia.
2. Department of Molecular Structural Biology, Max Planck Institute of Biochemistry, 82152 Martinsried, Germany.
3. School of Biological Sciences, University of Essex, Colchester CO4 3SQ, U.K.
4. CSIRO Biomedical Manufacturing, Melbourne, Victoria 3052, Australia
5. Thermo Fisher Scientific, 5651 GG Eindhoven, The Netherlands.
6. Department of Molecular Pharmacology and Experimental Therapeutics, Mayo Clinic, Scottsdale, Arizona 85259, U.S.A.
7. School of Biological Sciences, and Maurice Wilkins Centre for Molecular Biodiscovery, University of Auckland, Auckland, New Zealand.
8. School of Pharmacy, Fudan University, Shanghai 201203, China.

[†]Current address:
Novartis Institutes for Biomedical Research, Novartis Pharma AG, 4002 Basel, Switzerland

*These authors contributed equally to this work.

¶ To whom correspondence should be addressed:
Patrick Sexton, Patrick.sexton@monash.edu
Denise Wootten, denise.wootten@monash.edu

SUMMARY

Calcitonin gene-related peptide (CGRP) is a widely expressed neuropeptide that plays a major role in sensory neurotransmission. The CGRP receptor is a heterodimer of the calcitonin receptor-like receptor (CLR) class B G-protein-coupled receptor and the type 1 transmembrane domain protein, receptor activity modifying protein (RAMP) 1. Herein, we report the 3.3 Å structure of the human CGRP receptor in complex with CGRP and the Gs-protein heterotrimer determined by Volta phase plate cryo-electron microscopy. The RAMP transmembrane domain sits at the interface between transmembrane domains 3, 4 and 5 of CLR, and stabilises CLR extracellular loop 2. RAMP1 makes only limited direct interaction with CGRP, consistent with allosteric modulation of CLR as its key function. Molecular dynamics simulations indicate that RAMP1 provides stability to the receptor complex, particularly the location of the CLR extracellular domain. The work provides novel insight into the control of G-protein-coupled receptor function.

CGRP is a widely expressed sensory neuropeptide that has broad physiological functions. These include roles in modulation of metabolism, inflammatory response and blood pressure, as well as auditory nerve development and function[1-4]. It is a potent vasodilator that is released during neurogenic inflammation and contributes to the pathology of migraine. A first-in-class drug targeting the CGRP receptor was recently approved for treatment of this condition, and many other therapeutics are under development aimed at reducing CGRP activity[5]. In contrast, CGRP is protective in models of inflammatory bowel disease, and hypertension, and is a critical neuropeptide for development and modulation of auditory responses[1-4].

Receptor activity-modifying proteins (RAMPs), are essential accessory proteins for presentation of the class B calcitonin-like receptor (CLR) to the cell surface, and integral components of the phenotypically ascribed CGRP and adrenomedullin (AM) receptors, whereby CLR/RAMP1 engenders a selective response to CGRP, and CLR/RAMP2 or CLR/RAMP3, selective AM responses[6]. RAMPs are also partners for the calcitonin receptor (CTR), although not required for cell surface trafficking, they generate distinct amylin receptor (AMY) phenotypes[1]. Considerable cross talk between calcitonin-family peptides and receptors occurs, although current work has largely been restricted to how RAMPs impact cAMP signaling[1]. The three RAMPs each contain an ~100 amino acid, structured, N-terminal extracellular domain (ECD), a single TM domain and a short intracellular C-terminus. There is evidence that RAMPs co-evolved with GPCRs[7]; supporting this, we and others have shown that they can partner with numerous GPCRs, from all major subclasses, and are not exclusively partners for CLR and CTR[8-11].

Structures exist of heteromeric complexes of the isolated ECDs of RAMPs and CLR bound to C-terminal peptide fragments[12,13]. These structures have provided important but limited data on how RAMPs and CLR interact, and are unable to explain peptide selectivity. Thus, structures of full-length, active CGRP and AM receptor complexes are required to advance understanding.

Recent advances in cryo-electron microscopy (cryo-EM) have allowed full-length, class B GPCR, peptide agonist-bound structures to be elucidated in complex with their canonical Gs-protein heterotrimers[14-16]. These studies revealed class-specific, conserved, global conformational changes linked to receptor activation, and unexpected divergence in the modes of peptide binding, even within the same receptor[14-18]. In the current work, we have used Volta phase plate (VPP) cryo-EM to determine the structure of the human CGRP receptor complex, bound to its endogenous peptide agonist and canonical transducer at a

global resolution of 3.3 Å. This structure provides novel insights into how RAMPs interact with GPCRs and modulate their activity.

Structure determination

The CLR was modified to replace the native signal peptide with that of hemagglutinin (HA), and the addition of affinity tags bracketed by 3C cleavage sites at the N- and C-terminus (FLAG and His, respectively) (**Ext. Data Figure 1**). RAMP1 was modified to replace the native signal sequence with that of HA, followed by a FLAG epitope (**Ext. Data Figure 1**). These modifications did not alter receptor pharmacology (**Ext. Data Figure 2A**).

To form an active, G protein-coupled complex, the CLR and RAMP1 were co-expressed with Gαs, His-Gβ1, and Gγ2 in *Tni* insect cells and stimulated with 10 μM CGRP. A stabilised Gαs[15] was used enabling formation of a complex with improved stability[19]. Further complex stabilisation was achieved using camelid antibody Nb35[14-16]. The complex was treated with 3C enzyme to remove tags from CLR, solubilised in LMNG/cholesteryl hemisuccinate and then purified by sequential nickel and anti-FLAG columns, to ensure only RAMP1 bound complexes were present, and then further purified by SEC to yield a monodisperse complex that contained all components (**Ext. Data Figure 2B, 2C**).

Vitrified complexes were imaged in single particle cryo-EM using a Titan Krios microscope equipped with a VPP[20,21]. Following imaging (**Ext. Data Figure 3A**) and initial 2D classification (**Ext. Data Figure 3B**), 3D classification yielded a final map at a resolution of 3.3Å reconstructed from 407,000 particle projections (**Figure 1A; Ext. Data Figures 3C-3E; Supp. Information Table 1**). The cryo-EM density map exhibited well-resolved side chains, allowing confident rotamer placements for most amino acids within the peptide, receptor and RAMP TM domains and the G-protein (**Ext. Data Figure 4**). The RAMP and CLR ECDs had lower overall resolution, with discontinuous density for CLR ECD loop 1 and loop 5 (**Figure 1A; Ext. Data Figure 1; Ext. Data Figure 5**). Nonetheless, there was a strong correlation between the ECD EM density and the individual ECDs of either CLR or RAMP1 in deposited X-ray structure (PDB: 4RWG[12]). As such, these were rigid body fitted into the ECD density, with side chain adjustment where this was supported by density in the EM map. While individual ECDs from the X-ray structures had close approximation to the EM map, there were distinctions in the relative positioning of the CLR and RAMP1 ECDs in the two structures (**Ext. Data Figure 5**) that likely arise from anchoring constraints of the transmembrane domains (TMs) in the full-length structure. Continuous density was observed for the RAMP1 ECD and TM, including the unstructured linker domain, but not for the short C-terminal tail ($T144^{R}EGIV148^{R}$ (superscript R refers to residues within RAMP1)), indicating that this is mobile in the active receptor complex (**Figure 1**). There was robust density for most of the TM core and loops of CLR, excepting segments of ECL3 and ICL3 that were omitted from the model (**Figure 1; Ext. Data Figure 4**). Additional density was observed adjacent to the base of TMs 2 and 4 that may represent lipid interaction with CLR (**Ext. Data Figure 3G**). There was a relatively short helix 8 (H8), with no density for the CLR C-terminus beyond $Y402^{8.53}$ (receptor residues in superscript are defined using the class B numbering system[22,14]), while the far N-terminus of the ECD was also lacking density (**Figure 1; Ext. Data Figure 1**), indicating that these regions are also mobile. The CGRP peptide N-terminus ($A1^{P}$-$V23^{P}$ (P in superscript refers to peptide residues)) that binds within the receptor core, was well defined in the map, while the majority of side chains in the peptide C-terminus ($F27^{P}$-$F37^{P}$) that interact exclusively with receptor ECDs, were also supported by density (**Ext. Data Figure 4**). Similar to salmon calcitonin (sCT) in the Gs-coupled CTR[14] (**Figure 4**), there is a large kink in the peptide to enable interaction across the two receptor domains, with the CGRP linker

(K24^{P}-N26^{P}) poorly resolved in the map. Within the receptor core, side chains that had limited density were stubbed in the model (**Ext. Data Figure 1**). There was well resolved density for the G-protein heterotrimer across the receptor interface and between subunits. The α-helical domain of the α-subunit was only present in a small number of the 2D class averages and was masked out during map refinement. In general, the regions of lower resolution or lacking density were segments of the complex that exhibited higher mobility in MD simulations of the full complex (**Ext. Data Figure 6, Supp. Information Movies 1, 2**).

The RAMP1 CLR interface

The 2D class averages reveal that there is a single predominant orientation of the ECDs of the complex, relative to the CLR/RAMP core (**Ext. Data Figure 3B**). This contrasts to the variability in ECD orientation observed for the CTR[14]. RAMP1 makes extensive contacts with CLR with ~23% of its surface buried within this interface (**Figure 1B, 1C**). The extensive interface across the ECDs has been previously reported in X-ray crystal structures[12,23]. In contrast to predictions in published models of RAMPs with either CLR or CTR[24-27], the RAMP1 TM sits at an interface formed by CLR TMs 3, 4 and 5, with interactions of the upper half principally with TM5 (T288$^{5.33/ECL2}$, H289$^{5.34/ECL2}$, I293$^{5.38}$) (**Figure 2A, 2B)** and at the base with TM3 (L231$^{3.48}$, I235$^{3.52}$, T239$^{3.56}$, V243^{ICL2}) and TM4 (W254$^{4.44}$, Y255$^{4.45}$, L258$^{4.48}$, F262$^{4.52}$) (**Figure 2A, 2C**). These interactions were primarily van der Waals interactions, although there was potential for H-bond formation between Y255$^{4.45}$ and S141^{R}. D113^{R} in the membrane proximal segment of RAMP1 formed H-bonds with ECL2 residues proximal to CLR TM4 (Y278^{ECL2}), and TM5 (T288$^{5.33}$, H289$^{5.34}$) (**Figure 2B**). Alanine mutagenesis studies of CLR residues[28-33] revealed decreased CGRP potency for the Y278^{ECL2}, T288$^{5.33/ECL2}$ and W254$^{4.44}$ mutants with no impact on H289$^{5.34/ECL2}$, I293$^{5.38}$, T239$^{3.56}$, V243^{ICL2} and Y255$^{4.45}$ mutants[32,33], consistent with important but weak interactions between RAMP1 and CLR. Likewise, there was a small decrease in CGRP potency with D113^{R}A mutation indicating an indirect impact on CGRP peptide binding[34]. To understand the dynamics of the RAMP1/CLR interface we performed MD simulations, following modelling of missing amino acids and side chains into the full protein complex (**Ext. Data Figure 7A, 7B; Supp. Information Table 2; Supp. Information Movie 1**); these confirmed the importance of interactions between D113^{R} and CLR ECL2 (**Ext. Data Figure 7A**). The simulations also predicted that E47^{ECD} formed persistent H-bond interactions with R112^{R}, in addition to H-bonds to the backbone of G108^{R} and Ala110^{R} in the linker region. R112^{R} was also predicted to form less frequent H-bonds with D90^{ECD} but may maintain more persistent ionic interactions; collectively these interactions likely contribute to the limited mobility of the RAMP1 linker and stable positioning of the ECDs relative to the receptor core (**Ext. Data Figure 7A; Supp. Information Table 2; Supp. Information Movies 2, 3**). From the EM map, there were no resolved interactions between the RAMP and G-protein, however, there was no density for the RAMP1 C-tail. In MD simulations where the RAMP1 C-terminus was modelled transient interactions with ICL2, and the αN-helix of the Gα-protein were predicted, with potential interactions that could extend to ICL1 (**Supp. Information Table 2**). Nonetheless, this segment was highly mobile in the simulations.

The CGRP binding site

The CGRP peptide forms extensive interactions with the CLR/RAMP1 complex, with 61.5% of its surface buried. Intriguingly, the only direct contact between the peptide and RAMP1 occurs at the far C-terminus of the peptide, principally with the cluster of RAMP residues (F83^{R}-P85^{R}) that have been previously observed in isolated ECD structures[12] (**Figure 3A**). The N-terminal peptide loop that is constrained by C2^{P}-C7^{P} is deeply buried, extending into an amphipathic α-helix, until V23^{P}, that forms extensive van der Waal

interactions (**Figure 3D**). There are only limited H-bonds in the static structure between the peptide N-terminus and the CLR core; these include interactions between Y292$^{5.37}$ and the backbone of D3^{P}, between H295$^{5.40}$ and T6^{P}, and S286^{ECL2} and the backbone of H10^{P} (**Figure 3C, 3D**). Of these, only the interaction between H295$^{5.40}$ and T6^{P} is functionally important, with H295$^{5.40}$A reported to cause ~30-fold loss of CGRP potency in cAMP accumulation[28]. This amino acid is equivalent to H302$^{5.40}$ of the CTR that is predicted to form a H-bond with T6^{P} of sCT[14]. Alanine substitution of CGRP T6^{P} leads to ~80-fold loss of peptide potency[29], confirming the importance of this bond and other interactions. There are extensive interactions between the peptide and TM3, TM5 and ECL2 of CLR. Below H295$^{5.40}$, a series of amino acids that include I298$^{5.43}$, L302$^{5.47}$, M223$^{3.40}$ and Y227$^{3.44}$ form the bottom of the peptide binding pocket (**Figure 3C, 3D; Ext. Data Figure 8B**). Alanine substitution of T4^{P} leads to over 20-fold reduction in CGRP potency[29], however, it forms only limited interactions with the receptor. For this amino acid, side-chain to backbone interactions within the peptide that contribute to the loop fold and initiation of the peptide helix may underlie its functional importance. T9^{P} and H10^{P} pack within an extended cluster of residues that include T191$^{2.64}$, L195$^{2.68}$, H219$^{3.36}$, S286^{ECL2}, and I284^{ECL2} (**Figure 3C; Ext. Data Figure 8B**). With the exception of S286^{ECL2}, alanine mutation of these residues caused marked impairment in CGRP signalling[28,30-32] (**Ext. Data Figure 8B**), with I284^{ECL2} and L195$^{2.68}$ forming a hydrophobic barrier that coincides with the exit of the peptide from the receptor core (**Ext. Data Figure 8B**); MD simulations predict transient H-bond formation between T9^{P} and H219$^{3.36}$ (**Ext. Data Figure 9E; Supp. Information Table 3**). Alanine substitution of T9^{P} causes a 15-fold loss of CGRP potency[29], consistent with the importance of interaction of this side chain. While mutations to amino acids in the distal segment of ECL2 (S286^{ECL2}, D287^{ECL2}, H289^{ECL2}, L291$^{5.36}$) had relatively limited effects on CGRP potency[28] (**Ext. Data Figure 8B**), ECL2 conformation is critical to CGRP activation of its receptor, with R274$^{4.64}$ and, in particular, W283^{ECL2} mutation to alanine highly detrimental to CGRP signaling[32] (**Ext. Data Figure 8B**). These amino acids are critical to the stable packing of ECL2 in the active structure, similar to those observed in other active, class B GPCR structures[14-16]. There are only limited contacts between ECL1 and the peptide, the most prevalent being between L16^{P}, S17^{P} and A199^{ECL1}, N200^{ECL1}, Q202^{ECL1} and V205^{ECL1} (**Figure 3B; Ext. Data Figure 8B**). Q202^{ECL1} is within weak H-bond distance of the backbone oxygen of S17^{P} (**Ext. Data Figure 8B**), however, alanine mutation of Q202^{ECL1}, N200^{ECL1} or V205^{ECL1} had no impact on CGRP peptide potency, indicating limited importance of this domain for CGRP activity[30]. CLR and CTR have shorter ECL1 loops compared to the related glucagon (GCGR)[35], or glucagon-related peptide 1 receptor (GLP-1R)[15,16]. These receptors have longer TM2 and TM3 helices (**Ext. Data Figure 10A, 10B)** that interact with the extended helix of peptide agonists of these receptors[15,16,35]. In the EM map, there was no high-resolution density for ECL3 consistent with only limited interaction between CGRP and this receptor segment. This high mobility and lack of persistent interactions was also observed in our MD simulations (**Ext. Data Figure 9A-F); Supp. Information Table 3; Supp. Information Movie 2**), while previously published alanine mutagenesis provides additional support for the limited role of this domain in CGRP-mediated cAMP production[28,30] (**Ext. Data Figure 8B**).

V8^{P}, L12^{P} and L16^{P} lie on the same face of the peptide α-helix and sit deep within a groove formed by TMs 1 and 7, where they pack among multiple receptor residues. Alanine mutation of individual receptor amino acids within this groove have very little impact on CGRP-mediated cAMP production (**Ext. Data Figure 8B**), consistent with only weak contacts for individual amino acids. Nonetheless, alanine substitution of either L12^{P} or L16^{P} markedly impaired CGRP potency[36], indicating that the packing of the hydrophobic face of the peptide helix is critical for receptor activation.

In the EM structure, R11^{P} forms polar interactions with the backbone of peptide residues T4^{P} and C2^{P}, with potential salt-bridge interactions with D3^{P} and D366$^{7.39}$ of the receptor, and may contribute to stability of the peptide loop conformation (**Figure 3C**). In MD simulations, R11^{P} formed persistent H-bonds with D366$^{7.39}$, though such interactions are not observed in the EM map. R18^{P} is within salt-bridge distance to D287^{ECL2}, and D90^{ECD}, and forms a H-bond with D287^{ECL2} in nearly 25% of frames in the MD simulation (**Figure 3B, Ext Data Figure 9D, 9E**).

The resolution of the peptide C-terminus and receptor ECDs are lower than in the receptor core, and they were primarily modelled via rigid body fitting of the available x-ray structure (PDB: 4RWG[12]). To test the stability of interactions in the fully active structure, 6.4 μs MD simulations were run. Our data are consistent with the interactions previously reported in the isolated ECD structure[12], and are summarised in **Ext. Data Figure 9A-9F**, and **Supp. Information Table 3**. The main intermolecular interactions involved T30^{P} - D94^{ECD} (**Figure 3B, Ext. Data Figure 9E**), and F37^{P} (amide terminus) - T122^{ECD} (backbone atoms) (**Ext. Data Figure 9E**). There were no persistent hydrogen bonds between CGRP and RAMP1. The critical importance of interactions between the C-terminus of CGRP (F27^{P}-F37^{P}) and the CLR and RAMP1 ECDs for CGRP signaling has been highlighted by previous mutagenesis studies[12,23,34,37,38], and are illustrated in **Ext. Data Figure 8A**. The extent to which this is dependent upon the stability of the relative positioning of the ECD to the receptor core is unclear, but RAMP1 is a major contributor to the limited conformational flexibility of the CLR ECD domain (**Supp. Information Movie 3**).

Comparisons with the CTR structure

CTR is most closely related to CLR, and both can interact with RAMP1 to form a high affinity CGRP receptor[1]. As such, we compared our previously published structure of the sCT:CTR:Gs complex to the CGRP receptor complex. Due to the relatively limited resolution in density for the peptide binding domain and N-terminus of the CTR, comparisons were limited to the backbone structures in these regions. Overall, there was a high degree of similarity between the CLR and CTR structures, both exhibiting an extended TM1 α-helical stalk that interconnects the receptor core and ECD, and a similar organization of the upper segments of TM6 and TM7, to accommodate the bulk of the cysteine-bridged loops of the peptides (**Figure 4A**).

The largest difference was in the orientation of the ECD relative to the receptor core (**Figure 4A, 4B**). Intriguingly, this located the C-terminus of the peptides at virtually equivalent positions, with the N-terminal activation domain of the peptides also occupying a similar binding cavity (**Figure 4B**). Within the receptor core, there was an inward movement at the apex of TM5 of the CLR relative to CTR by ~2 Å, that is likely a product of the RAMP1 interaction with this domain (**Figure 4C**). There was a high degree of sequence conservation between CLR and CTR for the residues that contacted the RAMP (**Figure 4D**), which may explain the similar broad specificity for RAMP interaction of these receptors. We previously reported that, in simulations of the CTR bound to human CT (hCT) versus sCT, there was a surprising destabilization of ECL2 for hCT relative to the sCT bound receptor that was indicative of a role for conformational dynamics of this receptor domain in ligand interaction and efficacy[18]. The interactions of RAMP1 with ECL2 may therefore contribute to peptide selectivity and/or efficacy.

At the base of the receptor, the structured H8 of CLR was much shorter than that of CTR (**Figure 4A**), and consequently has more limited interaction with the Gβ subunit. Nonetheless, truncation studies of the CTR C-terminus indicated that only the segment that is also present in the CGRP receptor structure was functionally important for Gs

mediated signaling[14]. Perhaps more relevant, although the Gs-Ras α–H5 is aligned between the two structures, there are differences in the G-protein, particularly with respect to the positioning of the Gs-Ras α-N helix, which are propagated across the β- and γ-subunits (**Figure 4E**).

Broader comparison of Gs-protein interactions to include the active Gs-protein-coupled structures of the glucagon-like peptide-1 receptor (GLP-1R) bound to either exendin-P5 (ExP5)[15] or GLP-1[16] (**Ext. Data Figure 10A, 10B**), also revealed differences in the relative positioning of the Gs-protein, however, this was principally due to translational differences in the engagement of the receptors and the α-H5 (**Ext. Data Figure 10C**), with strong overlap in the backbone of the Gα subunit when these are aligned (**Ext. Data Figure 10D**). ICL2 of CLR and CTR are longer than their GLP-1R counter parts, and there is an ~2 Å greater outward movement of the base of TM6 of CLR and CTR compared to the GLP-1R (**Ext. Data Figure 10A**); these dissimilarities likely account for the translational differences in engagement of the Gs-protein by GLP-1R.

Stability of the complex in the absence of RAMP1

To help understand the contribution of RAMP1 to CGRP receptor function we performed MD simulations of the complex in the presence and absence of RAMP1. The orientation of the CLR ECD remains relatively stable during CLR-CGRP-RAMP1-Gαβγ-Nb35 (6.4 μs), and CLR-CGRP-RAMP1-miniGα (2 μs) MD simulations, but not during CLR-CGRP-miniGα (2 μs) MD simulations, as shown in **Supp. Information Movies 1-3**. In the absence of RAMP1, only CGRP and TM1, with its extension, hold the ECD in place relative to the TM domain. The N-terminal region ($A1^{P}$ – $R18^{P}$) of CGRP is stable (**Supp. Information Movie 2**), even in the absence of RAMP1, but the C-terminal region is affected by the mobility of the CLR ECD and is much more mobile in the absence of RAMP1 (**Ext. Data Figure 6; Supp. Information Movie 3**). A consequence of this C-terminal mobility in the absence of RAMP1 is reduced persistence of H-bonds formed by CGRP in this region, as shown in **Supp. Information Table 4**.

RAMP1 provides additional stability to ECL2, a major contact point for CGRP, even though this loop is relatively stable even in the absence of RAMP1. In the MD in the absence of RAMP1, there is a marked reduction in the persistence of H-bonds between $R274^{4.64}$ and $D280^{ECL2}$ (**Supp. Information Table 5**). In the cryo-EM structure, these two residues are able to form a salt-bridge interaction, and the stability of this interaction in the presence of RAMP1 is likely to impact on signal propagation. Indeed, mutagenesis of either of these residues greatly impacts CGRP mediated cAMP signalling[28,32]. RAMP1 interaction does not impact the mobility of ECL1 and ICL3, and indeed there is no direct contact between the receptor and RAMP in these regions. The least mobile points of each TM generally correspond to point of helix intersection; for TM3 this is in the vicinity of $Y227^{3.44}$, which provides a deep stable contact point for CGRP.

It is important to note that, while these simulations provide insight into the contribution of RAMP1 to the preformed active complex, this complex does not form in the absence of RAMP, even where CLR is present at the cell surface[6], indicating that the CLR/RAMP1 interaction is also critical for initial peptide binding and presentation to the receptor core.

In conclusion, the VPP cryo-EM structure of the CGRP-CLR-RAMP1-Gs complex provides unique insight into the organisation of functionally important heteromeric GPCR complexes. The RAMP1 causes marked stabilisation of the CLR ECD, and thus plays a critical role in ligand presentation to the receptor core. It further enhances stability of the TM domain interface and ECL2 that are important for propagation of peptide-induced

346 signalling. This study provides a framework for the development of novel therapeutics that
347 target the CGRP system.
348
349
350
351

352 **REFERENCES**

353 1. Hay, D. L., Garelja, M. L., Poyner, D. R., & Walker, C. S. Update on the
354 pharmacology of calcitonin/CGRP family of peptides: IUPHAR Review 25. *Br. J.*
355 *Pharmacol.* **175**, 3-17 (2018).
356 2. Russell, F. A., King, R., Smillie, S. J., Kodji, X., & Brain, S. D. Calcitonin gene-
357 related peptide: physiology and pathophysiology. *Physiol. Rev.* **94**, 1099-1142
358 (2014).
359 3. Dickerson, I. M., Bussey-Gaborski, R., Holt, J. C., Jordan, P. M., & Luebke, A. E.
360 Maturation of suprathreshold auditory nerve activity involves cochlear CGRP-
361 receptor complex formation. *Physiol. Rep.* **4** (2016).
362 4. Walker, C. S. *et al.* Mice lacking the neuropeptide alpha-calcitonin gene-related
363 peptide are protected against diet-induced obesity. *Endocrinology* **151**, 4257-4269
364 (2010).
365 5. Karsan, N., & Goadsby, P. J. Calcitonin gene-related peptide and migraine. *Curr.*
366 *Opin. Neurol*. **28**, 250-254 (2015).
367 6. McLatchie, L. M., *et al,* RAMPs regulate the transport and ligand specificity of the
368 calcitonin-receptor-like receptor. *Nature* 393, 333-339 (1998).
369 7. Barbash, S., Lorenzen, E., Persson, T., Huber, T., & Sakmar, T. P. GPCRs
370 coevolved with receptor activity-modifying proteins, RAMPs. *Proc. Natl. Acad. Sci.*
371 *U. S. A.* **114**, 12015-12020 (2017).
372 8. Hay, D. L., & Pioszak, A. A. Receptor Activity-Modifying Proteins (RAMPs): New
373 Insights and Roles. *Annu. Rev. Pharmacol. Toxicol.* **56**, 469-487 (2016).
374 9. Routledge, S. J., Ladds, G., & Poyner, D. R. The effects of RAMPs upon cell
375 signalling. *Mol. Cell Endocrinol.* **449**, 12-20 (2017).
376 10. Wootten, D. *et al.,* Receptor activity modifying proteins (RAMPs) interact with the
377 VPAC2 receptor and CRF1 receptors and modulate their function. *Br. J. Pharmacol.*
378 **168**, 822-834 (2013).
379 11. Christopoulos, A. *et al.* Novel receptor partners and function of receptor activity-
380 modifying proteins. *J. Biol. Chem.* **278**, 3293-3297 (2003).
381 12. Booe, J. M., Warner, M. L., Roehrkasse, A. M., & Pioszak, A. A. Structural Basis for
382 Receptor Activity-Modifying Protein-Dependent Selective Peptide Recognition by a
383 G Protein-Coupled Receptor. *Mol. Cell* **58**, 1040-1052 (2015).
384 13. Booe, J. M., *et al.* Probing the mechanism of receptor activity-modifying protein
385 modulation of GPCR ligand selectivity through rational design of potent
386 adrenomedullin and calcitonin gene-related peptide antagonists. *Mol. Pharmacol.*
387 **93**, 355-367 (2018).
388 14. Liang, Y. L. *et al.* Phase-plate cryo-EM structure of a class B GPCR-G-protein
389 complex. *Nature* **546**, 118-123 (2017).
390 15. Liang, Y. L. *et al.* Phase-plate cryo-EM structure of a biased agonist-bound human
391 GLP-1 receptor-Gs complex. *Nature* **555**, 121-125 (2018).
392 16. Zhang, Y. *et al.* Cryo-EM structure of the activated GLP-1 receptor in complex with
393 a G protein. *Nature* **546**, 248-253 (2017).
394 17. Wootten, D. *et al.* The extracellular rurface of the GLP-1 Receptor is a molecular
395 trigger for biased agonism. *Cell* **165**, 1632-1643 (2016).
396 18. Dal Maso, E. *et al.* Extracellular loops 2 and 3 of the calcitonin receptor selectively
397 modify agonist binding and efficacy. *Biochem. Pharmacol.* **150**, 214-244 (2018).
398 19. Liang, Y. L., *et al,* Nucleotide-free immobilized G proteins enhance formation of
399 agonist-GPCR-G protein complexes. *ACS Pharmacol Transl Sci* (in press).
400 20. Khoshouei, M. *et al.* Volta phase plate cryo-EM of the small protein complex Prx3.
401 *Nat. Commun.* **7**, 10534 (2016).

21. Khoshouei, M., Radjainia, M., Baumeister, W. & Danev, R. Cryo-EM structure of haemoglobin at 3.2 Å determined with the Volta phase plate. *Nat. Commun.* **8**, 16099 (2017)
22. Wootten, D., Simms, J., Miller, L. J., Christopoulos, A., & Sexton, P. M. Polar transmembrane interactions drive formation of ligand-specific and signal pathway-biased family B G protein-coupled receptor conformations. *Proc. Natl. Acad. Sci. U. S. A.* **110**, 5211-5216 (2013).
23. Ter Haar, E., *et al,* Crystal structure of the ectodomain complex of the CGRP receptor, a class-B GPCR, reveals the site of drug antagonism. *Structure* **18**, 1083-1093 (2010).
24. Watkins, H. A., *et al.,* Receptor activity-modifying proteins 2 and 3 generate adrenomedullin receptor subtypes with distinct molecular properties. *J. Biol. Chem.* **291**, 11657-11675 (2016).
25. Woolley, M. J., *et al.,* Receptor activity-modifying protein dependent and independent activation mechanisms in the coupling of calcitonin gene-related peptide and adrenomedullin receptors to Gs. *Biochem. Pharmacol.* **142**, 96-110 (2017).
26. Weston, C., *et al,* Receptor activity-modifying protein-directed G protein signaling specificity for the calcitonin gene-related peptide family of receptors. *J. Biol. Chem.* **291**, 21925-21944 (2016).
27. Bower, R. L., *et al.,* Molecular signature for receptor engagement in the metabolic peptide hormone amylin. *ACS Pharmacol. Transl. Sci.* (in press; DOI: 10.1021/acsptsci.8b00002).
28. Woolley, M. J., *et al,* Understanding the molecular functions of the second extracellular loop (ECL2) of the calcitonin gene-related peptide (CGRP) receptor using a comprehensive mutagenesis approach. *Mol. Cell Endocrinol.* **454**, 39-49 (2017).
29. Hay, D. L., *et al,* Structure-activity relationships of the N-terminus of calcitonin gene-related peptide: key roles of alanine-5 and threonine-6 in receptor activation. *Br. J. Pharmacol.* **171**, 415-426 (2014).
30. Barwell, J., Conner, A., & Poyner, D. R. Extracellular loops 1 and 3 and their associated transmembrane regions of the calcitonin receptor-like receptor are needed for CGRP receptor function. *Biochim. Biophys. Acta* **1813**, 1906-1916 (2011).
31. Vohra, S., *et al,* Similarity between class A and class B G-protein-coupled receptors exemplified through calcitonin gene-related peptide receptor modelling and mutagenesis studies. *J. R. Soc. Interface* **10**, 20120846 (2012).
32. Woolley, M. J., *et al,* The role of ECL2 in CGRP receptor activation: a combined modelling and experimental approach. *J. R. Soc. Interface* **10**, 20130589 (2013).
33. Conner, A. C., Simms, J., Howitt, S. G., Wheatley, M., & Poyner, D. R. The second intracellular loop of the calcitonin gene-related peptide receptor provides molecular determinants for signal transduction and cell surface expression. *J. Biol. Chem.* **281**, 1644-1651 (2006).
34. Simms, J., *et al,* Structure-function analysis of RAMP1 by alanine mutagenesis. *Biochemistry* **48**, 198-205 (2009).
35. Zhang, H., *et al*, Structure of the glucagon receptor in complex with a glucagon analogue. *Nature* **553**, 106-110 (2018).
36. Simms, J., *et al,* Photoaffinity cross-linking and unnatural amino acid mutagenesis reveal insights into calcitonin gene-related peptide binding to the calcitonin receptor-like receptor/receptor activity-modifying protein 1 (CLR/RAMP1) complex. *Biochemistry* (in press).

37. Garelja, M. L., *et al,* Receptor activity modifying proteins have limited effects on the Class B G protein-coupled receptor calcitonin receptor-like receptor stalk. *Biochemistry* **57**, 1410-1422 (2018).
38. Hay, D. L., Christopoulos, G., Christopoulos, A., & Sexton, P. M. Determinants of 1-piperidinecarboxamide, N-[2-[[5-amino-l-[[4-(4-pyridinyl)-l-piperazinyl]carbonyl]pentyl]amino]-1-[(3,5-dibromo-4-hydroxyphenyl)methyl]-2-oxoethyl]-4-(1,4-dihydro-2-oxo-3(2H)-quinazolinyl) (BIBN4096BS) affinity for calcitonin gene-related peptide and amylin receptors--the role of receptor activity modifying protein 1. *Mol. Pharmacol.* **70**, 1984-1991 (2006).
39. Johansson, E., *et al,* Type II turn of receptor-bound salmon calcitonin revealed by X-ray crystallography. *J. Biol. Chem.* **291**, 13689-13698 (2016).

ACKNOWLEDGEMENTS

The work was supported by the Monash University Ramaciotti Centre for Cryo-Electron Microscopy.

This work was supported by National Health and Medical Research Council of Australia (NHMRC) project grant (1120919), and NHMRC program grant (1055134). PMS and AC are NHMRC Principal and Senior Principal Research Fellows, respectively. DW is a NHMRC Career Development Fellow, and CK a NHMRC CJ Martin Fellow. AG is an Australian Research Council DECRA Fellow. DLH is a James Cook Research Fellow and is supported by the Marsden Fund (both Royal Society of New Zealand). CAR is a Royal Society Industry Fellowship and acknowledges support from the BBSRC (BB/M006883/1). We are grateful to George Christopoulos and Villy Julita for assay and technical support, Thomas Coudrat for initial homology modelling of CLR from the active CTR, and to Sebastian Furness, Peishen Zhao and David Thal for useful discussion.

The authors declare no competing financial or non-financial interests related to the research.

Reprints and permissions information is available at www.nature.com/reprints. Correspondence and requests for materials should be addressed to patrick.sexton@monash.edu or denise.wootten@monash.edu.

AUTHOR CONTRIBUTIONS

Y.L.L performed virus production, insect cell expression, purification, negative stain EM, data acquisition/analysis, prepared samples for cryo-EM, was responsible for model building and refinement, and assisted with manuscript preparation.
M.K performed cryo-sample preparation, phase-plate imaging, data collection, EM data processing and analysis, calculated the cryo-EM map and assisted with manuscript preparation.
G.D performed MD simulations and assisted in manuscript preparation.
A.G assisted with model building and refinement and contributed to manuscript preparation.
T.S.P assisted with model building and refinement and reviewed the manuscript.
C.K performed cell based assays and data analysis and reviewed the manuscript.
M.R performed preliminary screening imaging and reviewed the manuscript.
J.M.P and W.B organized and managed the Volta phase plate development project.
D.L.H provided insights into the CGRP receptor, assisted with data interpretation, and reviewed the manuscript.

L.J.M provided insights into class B GPCRs, assisted with data interpretation and reviewed the manuscript.
A.C assisted with data interpretation and manuscript preparation.
C.A.R. designed MD simulations, assisted in data interpretation and contributed to writing of the manuscript.
D.W was responsible for overall project strategy and management, data analysis and interpretation and contributed to writing of the manuscript.
P.M.S was responsible for overall project strategy and management, data interpretation and wrote the manuscript.

FIGURE LEGENDS

Figure 1 | The CGRP–CLR–RAMP1–Gs cryo-EM structure reveals molecular details of the RAMP-receptor interface. A, Left, 3.3 Å cryo-EM density map of the CGRP–CLR–RAMP1–Gs complex; the detergent micelle has been masked out for clarity. Middle, structure in ribbon representation after refinement in the cryo-EM map; CGRP, dark red; CLR, blue; RAMP1, dark orange; Gαs-Ras domain, gold; Gβ-subunit, cyan; Gγ-subunit, dark purple; Nb35, red. Right, cryo-EM density map coloured by local resolution (Å). **B-C**, CGRP receptor complex (ribbon representation coloured according to A), illustrating the extent of CLR interactions with other proteins in the complex (**B**), or the extent of RAMP1 interactions with other proteins in the complex (**C**), shown in mauve coloured surface representation. CGRP and RAMP1 form extensive contacts with CLR, with 61.5% and 23% of their surface buried, respectively.

Figure 2 | RAMP1 forms stable interactions with the CLR core and ECD. A, The CGRP-CLR-RAMP1 complex, with the interacting residues depicted in x-stick representation, with the backbone shown in ribbon representation. CGRP, dark red; CLR, blue; RAMP1, dark orange. Regions amplified in **B** (red) and **C** (blue) are boxed. **B**, RAMP1 interacts with ECL2 and the top of TM5 towards the extracellular face of the receptor. **C**, RAMP1 interacts with TM3 and TM4 towards the intracellular face of the receptor; interacting side chains are depicted in x-stick representation and the backbone in ribbon.

Figure 3 | The CGRP binding site. A, The CGRP interaction surface (amino acids within 5 Å) of CLR (blue) or RAMP1 (dark orange), illustrating how the peptide N-terminus is buried within CLR. CGRP is shown in dark red surface representation. **B-D**, amino acid side chains of CLR proximal to CGRP residues; amino acids are shown in x-stick with carbons in blue (CLR) or dark red (CGRP), and other atoms coloured by type. **B**, CGRP $L15^{P}$-$V23^{P}$ contact residues; $T30^{P}$ that forms two H-bonds with CLR $D94^{ECD}$ is also illustrated. **C**, CGRP $V8^{P}$-$G14^{P}$ contact residues. **D**, CGRP $A1^{P}$-$C7^{P}$ contact residues. There are very few H-bonds formed between the peptide N-terminus and CLR in the static structure.

Figure 4 | The CTR and CGRP receptor complexes display similar backbone conformations but have distinct conformations of the Gαs-Ras domain. A, Alignment of the CLR (blue ribbon)-RAMP1 (dark orange ribbon) and CTR (grey ribbon) structures; for the CTR the ECD is from the x-ray structure of the sCT-CTR x-ray structure (PDB: 5II0[39]), following rigid body fitting to the CTR EM map[14]. **B**, Zoom-in of the peptide binding sites; CGRP (dark red) and sCT (green) are shown as ribbon, CLR (blue) and CTR (grey) are shown as transparent ribbon. The circles highlight the similarities in position of the peptide N- (green) and C- (red) termini. RAMP1 has been omitted for clarity. **C**, Zoom-in illustrating distinctions in the upper segment of TM5 (red circle). **D**, Overlap in RAMP1 contact residues between CLR (blue x-stick) and CTR (grey x-stick). **E**, The Gαs-Ras-H5 is superimposed in the two structures, but the α-H1 helix is in a different orientation (red circle) and leads to distinctions in positioning of the Gβ and Gγ subunits. The CTR G protein is shown as grey ribbon, the CGRP receptor G protein as coloured ribbon; Gαs-Ras (gold), Gβ (cyan), Gγ (dark purple). Regions of the receptor structures that are missing in the PDB files are shown as dashed lines.

METHODS

Constructs. CLR was modified to include an N-terminal Flag tag epitope and a C-terminal 8xhistidine tag, both tags are removable by 3C protease cleavage. The construct was generated in both mammalian and insect cell expression vectors. RAMP1 was modified to include an N-terminal Flag tag epitope. For both constructs, the natural signal peptide was replaced with that of hemagglutinin to improve expression (**Ext. Data Figure 1**).

Insect cell expression. CLR, RAMP1, $DNG_{\alpha s}$[15], His6-tagged human $G_{\beta 1}$and $G_{\gamma 2}$were expressed in *Tni* insect cells (Expression systems) using baculovirus. Cell cultures were grown in ESF 921 serum-free media (Expression Systems) to a density of 4 million cells per ml and then infected with three separate baculoviruses at a ratio of 1:5:2:1 for CLR, RAMP1, $DNG_{\alpha s}$ and $G_{\beta 1\gamma 2}$. Culture was harvested by centrifugation 48 h post infection and cell pellet was stored at -80 °C.

Complex purification. Cell pellet was thawed in 20 mM HEPES pH 7.4, 50 mM NaCl, 2 mM $MgCl_2$ supplemented with cOmplete Protease Inhibitor Cocktail tablets (Roche). Complex formation was initiated by addition of 10 μM human αCGRP (Chinapeptide), Nb35–His (10 μg/mL), 3C protease (10 μg/mL) and Apyrase (25 mU/mL, NEB); the suspension was incubated for 1 h at room temperature. Membranes were collected by centrifugation at 30,000g for 30 min. Complexes from membranes were solubilized by 0.5% (w/v) lauryl maltose neopentyl glycol (LMNG, Anatrace) supplemented with 0.03% (w/v) cholesteryl hemisuccinate (CHS, Anatrace) for 2 h at 4 °C in the presence of 1 μM CGRP and apyrase (25 mU/mL, NEB). Insoluble material was removed by centrifugation at 30,000g for 30 min and the solubilized complex was immobilized by batch binding to NiNTA resin. The resin was packed into a glass column and washed with 20 column volumes of 20mM HEPES pH 7.4, 100 mM NaCl, 2 mM $MgCl_2$, 0.01% (w/v) LMNG and 0.006% (w/v) CHS, 1μM CGRP, before bound material was eluted in buffer containing 250 mM imidazole. The NiNTA purified fraction was immobilized by batch binding to M1 anti-FLAG affinity resin in the presence of 3 mM CaCl2. The resin was packed into a glass column and washed with 20 column volumes of 20 mM HEPES pH 7.4, 100 mM NaCl, 2 mM $MgCl_2$, 3 mM $CaCl_2$, 1 μM CGRP, 0.01% (w/v) LMNG and 0.006% (w/v) CHS before bound material was eluted in buffer containing 5 mM EGTA and 0.1 mg/mL FLAG peptide. The complex was then concentrated using an Amicon Ultra Centrifugal Filter (MWCO 100 kDa) and subjected to size-exclusion chromatography on a Superose 6 Increase 10/300 column (GE Healthcare) that was pre-equilibrated with 20 mM HEPES pH 7.4, 100 mM NaCl, 2 mM $MgCl_2$, 1 μM CGRP, 0.01% (w/v) LMNG and 0.006% (w/v) CHS. Eluted fractions consisting of receptor and G-protein complex were pooled and concentrated. Final yield of purified complex was approximately 0.3 mg per liter of insect cell culture.

SDS–PAGE and western blot analysis. Sample collected from size-exclusion chromatography was analyzed by SDS–PAGE and Western blot as previously described[15]. For SDS–PAGE, precast gradient TGX gels (Bio-Rad) were used. The final SEC elution peak was stained by Instant Blue (Expedeon).

Modelling into EM density. An initial template for CLR was generated by homology modelling on template cryo-EM structure of hCTR (PDB-5UZ7)[14], performed with the Molsoft ICM modelling software[40]. Manual adjustment and rebuilding was performed in COOT[41]. Due to limited density in CLR and RAMP1 ECD regions, we used the high-

resolution X-ray crystal structure (PDB-4RWG)[12] for modelling. ECDs of CLR and RAMP1 were, separately, rigid body fitted into density prior to the final iteration of global refinement. $DNG_{\alpha s}$, $G_{\beta 1}$, $G_{\gamma 2}$ and Nb35 models were taken from the GLP1R-Gs-ExP5 structure (PDB-6B3J)[15]. The CGRP peptide and RAMP1 TM were modeled manually. The final model was subjected to global refinement and minimization in real space using the module 'phenix.real_space_refine' in PHENIX[42]. Validation was performed in MolProbity[43].

Preparation of vitrified specimen. EM grids (Quantifoil, Großlöbichau, Germany, 200 mesh copper R1.2/1.3) were glow discharged for 30 s using Harrick plasma cleaner (Harrick, Ithaca, NY). 4 µl of sample was applied on the grid in the Vitrobot Mark IV chamber (Thermo Fisher Scientific, Waltham, MA). The chamber of Vitrobot was set to 100% humidity at 4 °C. The sample was blotted for 4.5 s with blot force of 20 and then plunged into propane-ethane mixture (37% ethane and 63% propane).

Data acquisition. Data set was collected on a Thermo Fisher Scientific Titan Krios microscope operated at 300 kV (FEI, Hillsboro, OR) equipped with a Gatan Quantum energy filter, a Gatan K2 summit direct electron camera (Gatan, Pleasanton, CA) and a Volta phase plate (Thermo Fisher Scientific). Movies were taken in EFTEM nanoprobe mode, with 50 µm C2 aperture, at a calibrated magnification of 47170 corresponding to a magnified pixel size of 1.06 Å. Each movie comprises 50 sub frames with a total dose of 50 e-/Å^2, exposure time was 13 s with the dose rate of 4.8 e-/pix/s on the detector. Data acquisition was done using SerialEM software at -600 nm defocus[44].

Data processing. 3180 movies were collected and subjected for motion correction using MotionCor2[45]. CTF estimation was done using Gctf software[46] on non-dose-weighted micrographs. The particles were picked using Gautomatch (developed by Dr Kai Zhang, MRC Laboratory of Molecular Biology, Cambridge, UK, http://www.mrc-lmb.cam.ac.uk/kzhang/Gautomatch/). An initial model was made using the common-line approach in EMAN2[47] based on automatically picked few micrographs and using the common-line approach. The particles were extracted in RELION 2.01b1[48] using a box size of 200 pixels. 1,205,000 picked particles were subjected to 2D classification with 100 classes, followed by 3D classification. After selecting the best-looking class, with 407,000 particles, 3D auto-refinement was performed in RELION 2.01b1. The final map was sharpened with a B-factor of -50 Å^2. The processing workflow is outlined in **Ext. Data Figure 3C**. Model overfitting was evaluated by randomly displacing all atoms by 0.5Å and refined against one cryo-EM half map. FSC curves were calculated between the resulting model and the half map used for refinement, the resulting model and the other half map for cross validation, and the final refined model and the full map (**Ext. Data Figure 3F**).

Mammalian cell cAMP assays. Cos7 cells, which were confirmed to be free from mycoplasma, were transfected in suspension in 96 well plates (10,000 cells/well) with 50ng CLR + 50ng human RAMP1 using 600ng PEI. The transfection was performed in 5% FBS DMEM, 200uL total volume per well and cells were incubated for 48 h at 37°C, 5% CO_2. cAMP detection was performed as previously described[49]. All values were converted to cAMP concentration using a cAMP standard curve performed in parallel and data were subsequently normalized to the response of 100 µM forskolin.

Conformational clustering of CGRP ECL3 and the RAMP1. The missing loops throughout CLR were generated using PLOP[50], which has been shown to be effective in generating GPCR loop conformations[51]. The missing side chains were iteratively optimized to convergence using PLOP. In addition, in order to enhance the conformational sampling of ECL3, which is likely to interact with the CGRP peptide, a preliminary clustering of 4000

671 different loop models generated using Modeller 9.16[52] was performed by means of the
672 Clustering VMD plugin (available at http://physiology.med.cornell.edu/
673 faculty/hweinstein/vmdplugins/clustering/). Conformational clustering was based on the
674 coordinates of side chains belonging to residues W354$^{6.58}$, R355$^{6.59}$, P356^{ECL3}, E357^{ECL3},
675 K359^{ECL3}, I360^{ECL3}, A361^{ECL3} and E362^{ECL3}. A total of 10 clusters were generated with a
676 Root Mean Standard Deviation (RMSD) cut off value of 3 Å and a representative structure
677 with a low Distributed Optimized Potential Energy (DOPE) score from the four most
678 populated ensembles was extracted and prepared for molecular dynamics simulations.
679 A similar approach was employed for clustering the modelled RAMP1 C-terminus
680 (residues T144^{R}, - V148^{R}): the original PLOP generated conformation was combined with
681 each of the 4 initially selected ECL3 conformations, while the highly distinct RAMP1 C-
682 terminus orientation was arbitrarily combined with ECL3 conformation number 1.
683
684 **Molecular dynamics (MD) simulations.** A total of seven systems were prepared for MD
685 simulations with the CHARMM36 force field[53] (**Supp. Information Table 6**) using a
686 multistep procedure that combines python htmd[54] and tcl (Tool Command Language)
687 scripts. Hydrogen atoms were first added by means of the pdb2pqr[55] and propka[56]
688 software (considering a simulated pH of 7.0); the protonation of titratable side chains was
689 checked by visual inspection. CLR and RAMP1 were embedded in a square 116 Å x 116
690 Å 1-palmitoyl-2-oleyl-sn-glycerol-3-phospho-choline (POPC) bilayer (previously built by
691 using the VMD Membrane Builder plugin 1.1, at
692 http://www.ks.uiuc.edu/Research/vmd/plugins/membrane/) through an insertion method[57].
693 More precisely, the opportune receptor orientation was obtained by superposing CLR
694 coordinates on the CTR structure retrieved from the OPM database[58]. Lipids overlapping
695 the receptor TMs bundle and the RAMP1 were removed and TIP3P water molecules[59]
696 were added to the simulation box (116 Å x 116 Å x 185 Å) by means of the VMD Solvate
697 plugin 1.5 (Solvate Plugin, Version 1.5. at
698 <http://www.ks.uiuc.edu/Research/vmd/plugins/solvate/). Overall charge neutrality was
699 finally reached by adding Na^{+}/Cl^{-} counter ions (final ionic strength of 0.150 M), using the
700 VMD Autoionize plugin 1.3 (Autoionize Plugin, Version 1.3. at
701 <http://www.ks.uiuc.edu/Research/vmd/plugins/autoionize/).
702 In order to evaluate the influence exerted by RAMP1 on the CGRP-CLR complex,
703 two simplified systems were embedded in a 96 Å x 96 Å POPC bilayers and solvated as
704 described above: one was composed by CLR-CGRP-RAMP1 and the C-terminus
705 (residues N371^{G} - L394^{G}) of the G-protein α subunit (CLR-CGRP-RAMP1-G-protein$_{(\alpha_{371-}}$
706 $_{394})$), while the other system was formed by CLR-CGRP and the C-terminus of the G-
707 protein α subunit (CLR-CGRP-G-protein$_{(\alpha_{371-394})}$); the original PLOP generated
708 conformations of CLR and RAMP1 were used.
709
710 **Systems equilibration and MD settings.** The MD engine ACEMD[60] was employed for
711 both the equilibration and productive simulations. Equilibration was achieved in isothermal-
712 isobaric conditions (NPT) using the Berendsen barostat[61] (target pressure 1 atm) and the
713 Langevin thermostat[62] (target temperature 300 K) with a low damping of 1 ps^{-1}. A three-
714 stage procedure was performed (integration time step of 2 fs): first, clashes between
715 protein and lipid atoms were reduced through 2500 conjugate-gradient minimization steps,
716 then a 2 ns long MD simulation was run with a positional constraint of 1 kcal mol^{-1} $Å^{-2}$ on
717 protein and lipid phosphorus atoms. During the second stage, 40 ns of MD simulation were
718 performed constraining only the protein atoms, while in the last equilibration stage,
719 positional constraints were applied only to the protein backbone alpha carbons, for a
720 further 5 ns.
721 **Supp. Information Table 6** summarizes all the simulations performed. Trajectories
722 were computed with an integration time step of 4 fs in the canonical ensemble (NVT) at

723 300 K, using a thermostat damping of 0.1 ps^{-1} and the M-SHAKE algorithm[63] to constrain
724 the bond lengths involving hydrogen atoms. The cut off distance for electrostatic
725 interactions was set at 9 Å, with a switching function applied beyond 7.5 Å. Long range
726 Coulomb interactions were handled using the particle mesh Ewald summation method
727 (PME)[64] by setting the mesh spacing to 1.0 Å.
728
729 **MD analysis.** Atomic contacts, hydrogen bonds and Root Mean Square Fluctuation
730 (RMSF) were computed using VMD[65]. A contact was considered productive if the distance
731 between two atoms was lower than 3.5 Å. For hydrogen bond detection, a donor-acceptor
732 distance of 3 Å and an angle value of 160° were set as geometrical cut-offs. The hydrogen
733 bond persistence is defined as the number of frames in which the H-Bond is formed
734 divided by the total number of frames times 100. The RAMP1 influence on van der Walls
735 contacts and hydrogen bonds was evaluated by computing the numerical difference
736 between the total numbers of contacts/hydrogen bonds between each CLR and CGRP
737 side chain during the simulations in presence and absence of RAMP1.
738
739 **Data availability.** All relevant data are available from the authors and/or included in the
740 manuscript or Supplementary Information. Atomic coordinates and the cryo-EM density
741 map have been deposited in the Protein Data Bank (PDB) under accession number 6E3Y
742 and EMDB entry ID EMD-8978.
743
744 **Extended Data Figure 1 | Amino acid sequences of the CGRP peptide, CLR and**
745 **RAMP1 constructs use for determination of structure.** The sequences are annotated
746 to denote the location of the HA signal sequence (red highlight), C3 cleavage sites (grey
747 highlight), FLAG (dark olive-green highlight) and His tags (purple highlight). The
748 substituted sequences of the native proteins are listed above the construct sequences and
749 highlighted in blue. Transmembrane helical domains in CLR and RAMP1 are boxed and
750 highlighted in green. Segments of the proteins that were not resolved in the EM map are
751 highlighted in yellow. Amino acids for which backbone density was present but limited side
752 chain density, were stubbed in the model; these are bolded in red in the sequences.
753
754 **Extended Data Figure 2 | CGRP receptor pharmacology and purification of the**
755 **CGRP-CLR-RAMP1-Gs complex. A**; Pharmacology of untagged CLR-RAMP1 (WT CLR-
756 RAMP1) and the purification construct (HA–FLAG-CLR, FLAG-RAMP1), in CGRP-
757 mediated cAMP accumulation assays performed in transiently transfected Cos7 cells (N=5
758 separate experiments with triplicate repeats; mean + s.e.). **B**; Expression and purification
759 strategy. **C**; Final size exclusion chromatography (SEC) elution profile of the complex. **D**;
760 SDS–PAGE/Coomassie blue stain of the SEC peak, demonstrating presence of each of
761 the components of the complex.
762
763 **Extended Data Figure 3 | Volta phase plate imaging of the CGRP–CLR–RAMP1-Gs**
764 **heterotrimer complex. A**; Volta phase plate micrograph of the complex (representative of
765 3,180). High-contrast phase plate imaging facilitates robust particle selection despite low
766 defocus and tight packing of particles. **B**; RELION 2D class averages. **C**; Workflow for map
767 refinement. **D**; Final 3D EM map calculated in RELION after auto-refinement and map
768 sharpening. **E**; 'gold standard' Fourier shell correlation (FSC) curve; the overall nominal
769 resolution is 3.26 Å. **F**; Model overfitting was evaluated by randomly displacing all atoms
770 by 0.5Å and refined against one cryo-EM half map. FSC curves were calculated between
771 the resulting model and the half map used for refinement (green); the resulting model and
772 the other half map for cross validation (red), and the final refined model and the full map
773 (blue). **G**; Potential lipid interaction with the base of TM4 and TM2 of CLR.
774

Extended Data Figure 4 | Atomic resolution model of the CGRP–CLR–RAMP1-Gs heterotrimer in the cryo-EM density map. EM density map and model are shown for all seven transmembrane helices and H8 of the receptor, the CGRP peptide (excepting the $K24^{P}A25^{P}N26^{P}$ sequence that was not resolved in the map), the RAMP TM and each of the RAMP ECD helices; there was only limited side chain density for RAMP1 H1, with side chains modeled from rigid body fitting of the RAMP1 ECD in PDB: 4RWG[12]. Also illustrated are the N-terminal (αH1) and C-terminal (αH5) α-helices of the Gαs-Ras domain.

Extended Data Figure 5 | Comparison of the backbone position of the ECD of CLR (blue ribbon) and RAMP1 (orange ribbon) from the modelled, active complex, and the structure of the isolated CLR-RAMP1 ECD complex solved by x-ray crystallography[12] (light grey ribbon). The structures were aligned on the RAMP1 ECD. The CLR loops (Loops 1 – 5) are annotated. The CLR loop1 and loop 5 sequences that were not resolved in the EM map are indicated by dotted black arrows. Differences in the backbone position of CLR loops 4 and 5 are indicated in blue (active complex) and grey (isolated ECD complex) dotted arrows. The location of the CGRP peptide is shown in dark red.

Extended Data Figure 6 | Root mean square fluctuation (RMSF) for CGRP and CLR taken from the three simulations, namely CLR-CGRP-RAMP1-Gαβγ-Nb35 (black, 2.4 μs), CLR-CGRP-RAMP1-Gα(371-394) (purple, 2 μs) and CLR-CGRP-Gα(371-394) (blue, 2 μs). **A**; The CLR ECD region. **B**; the CLR TM region. **C**; CGRP (superposed on Thr^{6}-Ser^{17} and so valid for N-terminal half). In general, the missing segments in the EM density map correspond to regions of high RMSF and indeed the difficulty of fitting the ECD as a whole is linked to its high RMSF (**A; Supp. Information Movies 2, 3**). The ECD missing segments ($D55^{ECD}$-$V63^{ECD}$) and ($Q107^{ECD}$-$G109^{ECD}$) correspond to external loop regions furthest removed from the TM domain. Despite their polar nature they displayed no persistent interactions during the MD simulations; $D55^{ECD}$-$V63^{ECD}$ displayed the largest backbone RMSF of 8Å, while $Q107^{ECD}$-$G109^{ECD}$ displayed a similarly high RMSF of 7.5 Å. The next highest RMSF peaks around $A79^{ECD}$-$G81^{ECD}$ and $P115^{ECD}$-$S117^{ECD}$ are just a little lower but are nonetheless resolved (**A**). Within the TM domain, ICL3 (H324-S328) and ECL3 (P356-E362) both contain missing residues and have a high RMSF above 4.5 Å (**B**). This region displays no persistent interactions during the MD simulations, although CGRP does interact to the proximal (non-missing) region of ECL3. The high RMSF values for ICL1 (3.6 Å) and ICL2 (3.6 Å) give rise to stubbed residues ($K167^{2.40}$) and $E248^{ICL2}$-$Q250^{ICL2}$) but the backbone is resolved. For CGRP, the peak in the RMSF around residue 26 (**C**) corresponds to the three highly mobile external residues ($Lys^{24}Asn^{25}Asn^{26}$) in the outward-facing loop that do not interact with CLR (**Ext. Data Figure 8**); these residues could not be placed from the electron density. These three CGRP residues form a hinge, enabling changes in the orientation of the CLR ECD, especially in the absence of RAMP1; the higher RMSF values C-terminal to this are an artefact of the superposition strategy and the two-domain nature of CLR but their relative values still hold. The high mobility of some of the extracellular loops is visible in movies (**Supp. Information Movies 1-3**).

Extended Data Figure 7 | RAMP1 makes extensive stable interactions with CLR. A; Hydrogen bonds between RAMP1 and CLR during MD simulations (6.4 μs). The total persistency is plotted onto the experimental structure according to a rainbow colour scale, with residues never involved in dark blue and residue highly involved in red. The receptor is shown as a bulky ribbon, the RAMP1 as a thin coloured ribbon and the peptide as a thin white ribbon. Key side chains are shown, but for intermittent hydrogen bonds the rotameric state has been modified to show an interaction. Residues forming an interaction network

are labelled with the same colour. Left, overall topology of the system. Right upper, zoom on the upper portion of the CLR TM domain and ECD; lower, view rotated by 90° on the z axis. H-bonds involving RAMP1-CLR residues $R112^{R}$-$E47^{ECD}$ and $D113^{R}$-$T288^{ECL2}$/$H289^{ECL2}$ are significant for linking the TM domain to the ECD and for stabilizing ECL2. Other H-bonds implicated in stabilizing the CLR and RAMP1 ECD interaction include $S107^{R}$-$E47^{ECD}$, $R102^{R}$-$D55^{ECD}$, $H97^{R}$- $Q50^{ECD}$, $D90^{R}$-$Y49^{ECD}$, $D71^{R}$-$R38^{ECD}$ and $E29^{R}$-$R119^{ECD}$; quantitative data on the persistence of H-bonds during the simulations are reported in **Supp. Information Table 2**. **B**; Contacts between RAMP1 and CLR during MD simulations (6.4 μs). The total persistency of a residue side chain is plotted onto the experimental structure according to a cyan-maroon colour scale, with residues never involved in cyan and residue highly involved in maroon. The peptide (italics, dashed line) is depicted as a thin ribbon, while the receptor (solid line) is shown as a bulky ribbon and transparent surface. Left, overall topology of the system. Upper right, the most persistent interactions involving RAMP residues and the CLR ECD, $W59^{R}$, $I63^{R}$, $Y66^{R}$, $H97^{R}$ and $I106^{R}$ help to anchor αH3 and the C-terminal RAMP1 regions of αH2 to (residues $M42^{ECD}$, $T43^{ECD}$, $Y46^{ECD}$, $Y49^{ECD}$, $Q50^{ECD}$, and $M53^{ECD}$, of the CLR ECD). Lower right, the most persistent hydrophobic interactions between the TM domains of RAMP1 and CLR, namely $I123^{R}$, $P126^{R}$, $T130^{R}$, $T134^{R}$, and $V137^{R}$ (plus $S141^{R}$) help to anchor the RAMP transmembrane helix to CLR (TM3-TM5; CLR residues $Y277^{ECL2}$, $H289^{ECL2}$, $A300^{5.45}$, $I235^{3.52}$, $F262^{4.52}$, $L258^{4.48}$ and $W254^{4.44}$).

Extended Data Figure 8 | Effect of alanine mutagenesis of CLR or RAMP1 on CGRP potency in cAMP accumulation assays. A; ECD alanine mutations. **B**; CLR core alanine mutations. Residues that have been mutated are displayed in x-stick format. Mutated residues with no effect on signalling are coloured off-white. Residues that have significantly altered CGRP signaling[12,23,28,30-32,34,37,38] are also highlighted in transparent CPK representation, coloured according to magnitude of effect. <10 fold, yellow; 10-100 fold, dark orange; 100-1000 fold, red; >1000 fold, black. The backbones of CLR and RAMP (solid lines) are displayed in transparent, off-white coloured ribbon. The CGRP peptide (dashed lines) is represented in x-stick format with carbon atoms in dark red and polar atoms coloured in red or blue.

Extended Data Figure 9 | CGRP makes extensive stable interactions with CLR. A-D; Distances between CGRP and CLR residues relevant to key hydrogen bonds. The x-axis denotes sampling time for the 16 merged MD replicas of the whole system (each replica is separated by vertical dashed lines). **A**; Distance between the peptide $D3^{P}$ carboxylic carbon and receptor $R355^{6.59}$ guanidinium carbon. **B**; distance between the peptide $T6^{P}$ side chain oxygen atom and the receptor $H295^{5.40}$ side chain nitrogen atoms (for each frame, the closest nitrogen to $T6^{P}$ was considered). **C**; Distance between the peptide $R11^{P}$ guanidinium carbon and the receptor $D366^{7.39}$ carboxylic carbon. **D**; Distance between peptide $R18^{P}$ guanidinium carbon and receptor $D287^{ECL2}$ carboxylic carbon. In most cases the distances corresponding to hydrogen bond formation are slightly longer than the standard 2.8 Å. **E**; H-bonds between CGRP and CLR during MD simulations (6.4 μs). The total persistency of a residue side chain is plotted onto the experimental structure according to a rainbow colour scale, with residues never involved in blue and residues highly involved in red. The peptide (italics, dashed line) is depicted as thin ribbon, while the receptor (solid line) is shown as bulky ribbon. Key side chains are shown, but for intermittent H-bonds the rotameric state has been modified to show an interaction. Residues forming an interaction network are labelled with the same colour. Lower panel, H-bonds between the CGRP N-terminus and the TM bundle of CLR. Upper panel, H-bonds between the CGRP C-terminus and the ECD of CLR; quantitative data on the persistence of H-bonds during the simulations are reported in **Supp. Information Table 3.**

F; Contacts between CGRP and CLR / RAMP1 during MD simulations (6.4 μs). The total persistency of a residue side chain is plotted onto the experimental structure according to a cyan-maroon colour scale, with residues never involved in cyan and residue highly involved in maroon. The peptide (italics, dashed line) is depicted as a thin ribbon, while the receptor (solid line) is shown as a bulky ribbon and transparent surface. Left, contacts between the N-terminus of CGRP and the TM bundle of the CLR: highly persistent hydrophobic interactions characterize peptide residues $L12^{P}$, $L16^{P}$, $H10^{P}$ and receptor residues $L195^{2.68}$, $A138^{1.36}$ and $H295^{5.40}$. Right, contacts between the C-terminus of CGRP and the ECD of CLR; highly persistent contacts characterize peptide residues $V32^{P}$, $T30^{P}$, $F37^{P}$ and receptor residues $Q93^{ECD}$ and $W72^{ECD}$. RAMP1 residues $F83^{R}$, $W84^{R}$ are mainly engaged by CGRP residue $F37^{P}$.

Extended Data Figure 10 | Class B GPCRs display similar active state conformations. A-B; Alignment of the CGRP-CLR-RAMP1, sCT-CTR, ExP5-GLP-1R and GLP-1-GLP1R structures (aligned on the TM domains). Regions of divergence between CLR/CTR and GLP-1R are circled. In **A**, RAMP1 has been omitted for clarity. **C**; Position of the Gαs-Ras domain in the CTR (left), GLP-1R (GLP-1 bound; middle) and GLP-1R (ExP5 bound; right). The receptor TMs were aligned. Only the CLR (blue) and RAMP1 (orange) are displayed for clarity. **D**; The Gαs-Ras domain from each of the four structures, aligned according to the Gαs-Ras.

METHODS SPECIFIC REFERENCES

40. Abagyan, R. & Totrov, M. Biased probability Monte Carlo conformational searches and electrostatic calculations for peptides and proteins. *J. Mol. Biol.* **235**, 983-1002 (1994).
41. Emsley, P. & Cowtan, K. Coot: model-building tools for molecular graphics. *Acta Crystallogr. D Biol. Crystallogr.* **60**, 2126–2132 (2004).
42. Adams, P. D. *et al.* PHENIX: a comprehensive Python-based system for macromolecular structure solution. *Acta Crystallogr. D Biol. Crystallogr.* **66**, 213–221 (2010).
43. Chen, V. B. *et al.* MolProbity: all-atom structure validation for macromolecular crystallography. *Acta Crystallogr. D Biol. Crystallogr.* **66**, 12–21 (2010).
44. Mastronarde, D. N. Automated electron microscope tomography using robust prediction of specimen movements. *J. Struct. Biol.* **152**, 3651 (2005).
45. Zheng, S. Q. *et al.* MotionCor2: anisotropic correction of beam-induced motion for improved cryo-electron microscopy. *Nat. Methods* **14**, 331–332 (2017).
46. Zheng, K. Gctf: Real-time CTF determination and correction. *J. Struct. Biol.* **193**, 1-12 (2016).
47. Tang, G. et al. EMAN2: an extensible image processing suite for electron microscopy. *J. Struct. Biol.* **157**, 38–46 (2007).
48. Kimanius, D., Forsberg, B. O., Scheres, S. H. & Lindahl, E. Accelerated cryo-EM structure determination with parallelisation using GPUs in RELION-2. *Elife* **5**, e18722 (2016).
49. Hager, M. V., Clydesdale, L., Gellman, S. H., Sexton, P. M. & Wootten, D. Characterization of signal bias at the GLP-1 receptor induced by backbone modification of GLP-1. *Biochem. Pharmacol.* **136**, 99–108 (2017).
50. Jacobson, M. P. *et al.* A hierarchical approach to all-atom protein loop prediction. *Proteins* **55**, 351–367 (2004).
51. Goldfeld, D. A., Zhu, K., Beuming, T. & Friesner, R. A. Successful prediction of the intra- and extracellular loops of four G-protein-coupled receptors. *Proc. Natl. Acad. Sci. U. S. A.* **108**, 8275–8280 (2011).
52. Eswar, N. *et al.* Comparative protein structure modeling using Modeller. *Curr. Protoc. Bioinformatics* Chapter 5, Unit 5.6 (2006).
53. Huang, J. & MacKerell, A. D. CHARMM36 all-atom additive protein force field: validation based on comparison to NMR data. *J. Comput. Chem.* **34**, 2135–2145 (2013).
54. Doerr, S., Harvey, M. J., Noé, F. & De Fabritiis, G. HTMD: High-Throughput Molecular Dynamics for Molecular Discovery. *J. Chem. Theory Comput.* **12**, 1845–1852 (2016).
55. Dolinsky, T. J., Nielsen, J. E., McCammon, J. A. & Baker, N. A. PDB2PQR: an automated pipeline for the setup of Poisson-Boltzmann electrostatics calculations. *Nucleic Acids Res.* **32**, W665-7 (2004).
56. Olsson, M. H. M., Søndergaard, C. R., Rostkowski, M. & Jensen, J. H. PROPKA3: Consistent Treatment of Internal and Surface Residues in Empirical pK Predictions. *J. Chem. Theory Comput.* **7**, 525–537 (2011).
57. Sommer, B. Membrane Packing Problems: A short Review on computational Membrane Modeling Methods and Tools. *Comput. Struct. Biotechnol. J.* **5**, e201302014 (2013).
58. Lomize, M. A., Lomize, A. L., Pogozheva, I. D. & Mosberg, H. I. OPM: orientations of proteins in membranes database. *Bioinformatics* **22**, 623–625 (2006).

59. Jorgensen, W. L., Chandrasekhar, J., Madura, J. D., Impey, R. W. & Klein, M. L. Comparison of simple potential functions for simulating liquid water. *J. Chem. Phys.* **79**, 926 (1983).
60. Harvey, M. J., Giupponi, G. & Fabritiis, G. D. ACEMD: Accelerating Biomolecular Dynamics in the Microsecond Time Scale. *J. Chem. Theory Comput.* **5**, 1632–1639 (2009).
61. Berendsen, H. J. C., Postma, J. P. M., van Gunsteren, W. F., DiNola, A. & Haak, J. R. Molecular dynamics with coupling to an external bath. *J. Chem. Phys.* **81**, 3684 (1984).
62. Loncharich, R. J., Brooks, B. R. & Pastor, R. W. Langevin dynamics of peptides: the frictional dependence of isomerization rates of N-acetylalanyl-N'-methylamide. *Biopolymers* **32**, 523–535 (1992).
63. Kräutler, V., van Gunsteren, W. F. & Hünenberger, P. H. A fast SHAKE algorithm to solve distance constraint equations for small molecules in molecular dynamics simulations. *J. Comput. Chem.* **22**, 501–508 (2001).
64. Essmann, U. *et al.* A smooth particle mesh Ewald method. *J. Chem. Phys.* 103, 8577 (1995).
65. Humphrey, W., Dalke, A. & Schulten, K. VMD: visual molecular dynamics. *J. Mol. Graph.* **14**, 33–38, 27 (1996).

SUPPORTING INFORMATION

Supporting Information Table 1. A, PDB validation report. **B**, Cryo-EM data collection, refinement and validation statistics.

Supporting Information Table 2. Persistence of H-bonds and other contacts between RAMP1 and CLR in MD simulations.

Supporting Information Table 3. Persistence of H-bonds and other contacts between CGRP and CLR or RAMP1 in MD simulations.

Supporting Information Table 4. The difference in hydrogen bond formation between CGRP and CLR, during MD simulations performed on the CGRP-CLR-Gα(371-394) complex in the presence and absence of RAMP1.

Supporting Information Table 5. The difference in CLR intra-molecular hydrogen bonds formation in the presence or absence of RAMP1.

Supporting Information Table 6. Summary of all the MD simulations performed on the CLR-CGRP-RAMP1-G-protein.

Supporting Information Movie 1.
The CGRP (grey), CLR (green), RAMP1 (orange), G-protein (α subunit in blue, β subunit in red and γ subunit in yellow), Nb35 (maroon) complex simulated during a 400 ns long MD replica. Water molecules, ions and the lipid bilayer have been removed for clarity.

Supporting Information Movie 2.
Details of the extracellular TMs bundle during a 500 ns long MD replica, performed on the CGRP-CLR-RAMP1-G-protein complex. The hydrogen bonds formed between CGRP (orange), and CLR (cyan), and between CGRP (orange) and RAMP1 (green) are highlighted as dotted lines throughout the simulation.

Supporting Information Movie 3.
Comparison between two different 500 ns long MD simulations performed on: Left, CGRP (orange), CLR (green ribbon and transparent surface), RAMP1 (magenta ribbon and transparent surface), G-protein (371-394) complex. Right, CGRP (orange), CLR (green ribbon and transparent surface), G-protein (371-394) complex.

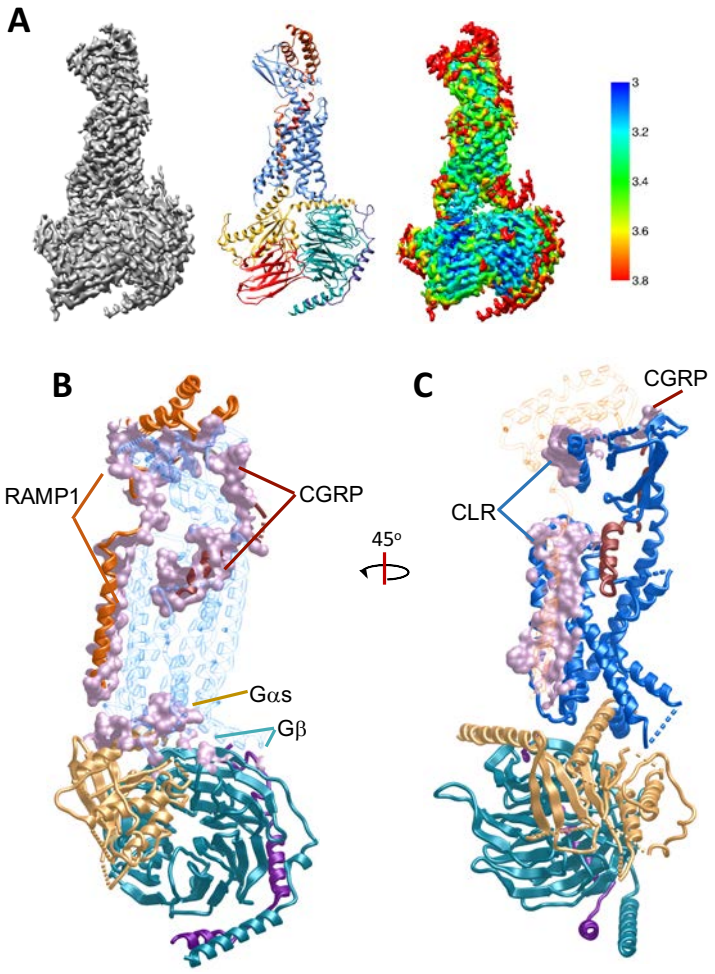
A
3
3.2
3.4
3.6
3.8
B
RAMP1
CGRP
Gαs
Gβ
45°
C
CGRP
CLR

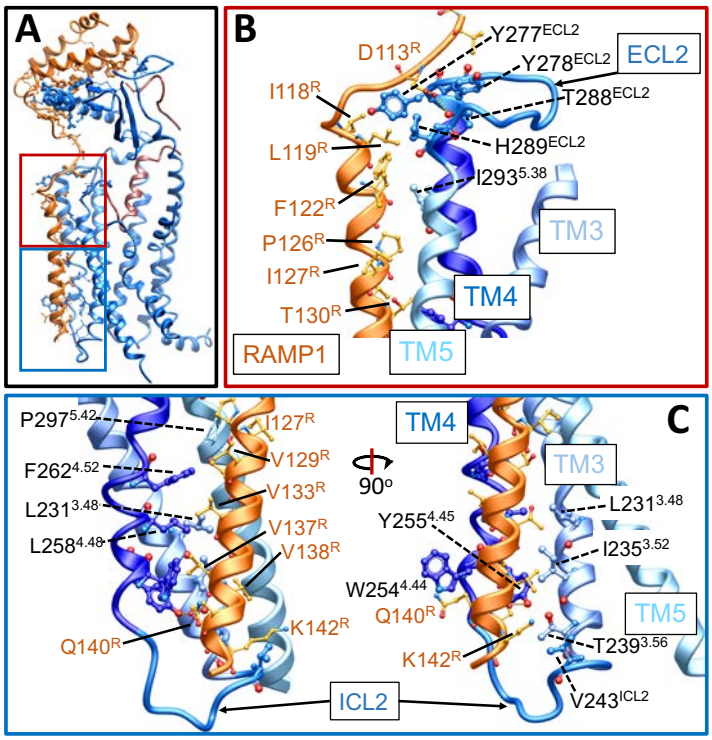
A
B
D113R
Y277ECL2
Y278ECL2
ECL2
I118R
T288ECL2
L119R
H289ECL2
I2935.38
F122R
TM3
P126R
I127R
TM4
T130R
RAMP1
TM5
C
P2975.42
I127R
TM4
F2624.52
V129R
90o
TM3
L2313.48
V133R
L2313.48
L2584.48
V137R
Y2554.45
V138R
I2353.52
W2544.44
Q140R
TM5
K142R
Q140R
T2393.56
K142R
ICL2
V243ICL2

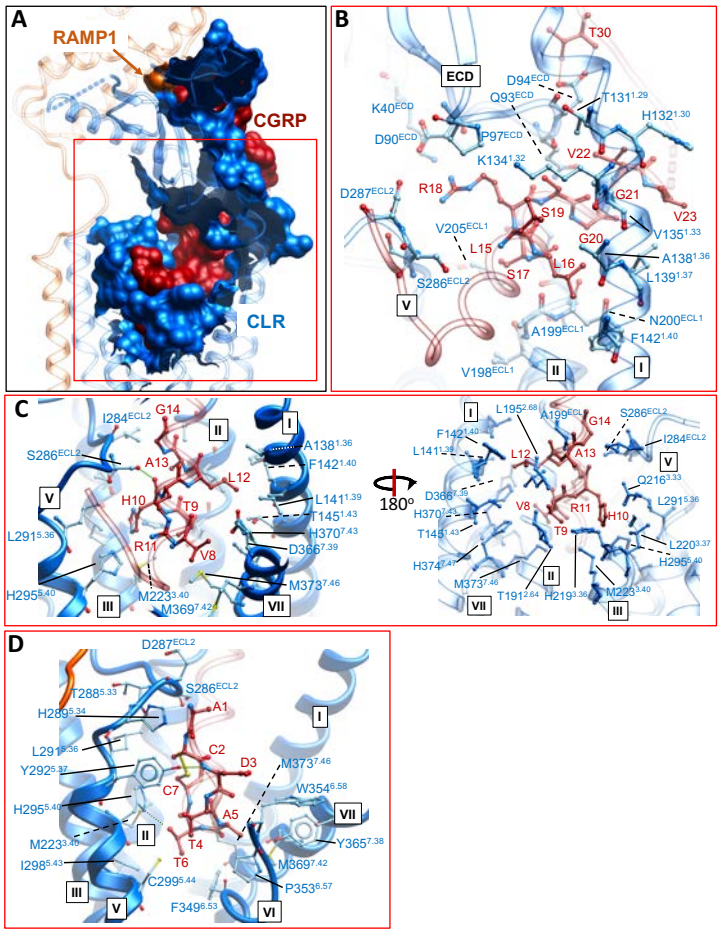
A
RAMP1
CGRP
CLR
B
ECD
T30
D94ECD
Q93ECD
T1311.29
K40ECD
H1321.30
D90ECD
P97ECD
V22
K1341.32
D287ECL2
R18
G21
S19
V23
V205ECL1
V1351.33
L15
G20
A1381.36
S286ECL2
S17
L16
L1391.37
V
N200ECL1
A199ECL1
F1421.40
V198ECL1
II
I
C
I284ECL2
G14
II
I
S286ECL2
A13
A1381.36
F1421.40
L12
V
H10
T9
L1411.39
T1451.43
L2915.36
H3707.43
R11
V8
D3667.39
H2955.40
M2233.40
M3737.46
M3697.42
III
VII
180°
L1952.68
A199ECL1
S286ECL2
F1421.40
G14
I284ECL2
L1411.39
L12
A13
V
Q2163.33
D3667.39
V8
R11
H10
L2915.36
H3707.43
T1451.43
T9
L2203.37
H2955.40
H3747.47
M3737.46
T1912.64
H2193.36
M2233.40
II
VII
III
D
D287ECL2
T2885.33
S286ECL2
A1
H2895.34
I
L2915.36
C2
D3
M3737.46
Y2925.37
C7
W3546.58
H2955.40
A5
VII
II
M2233.40
T4
Y3657.38
I2985.43
T6
M3697.42
III
C2995.44
P3536.57
V
F3496.53
VI

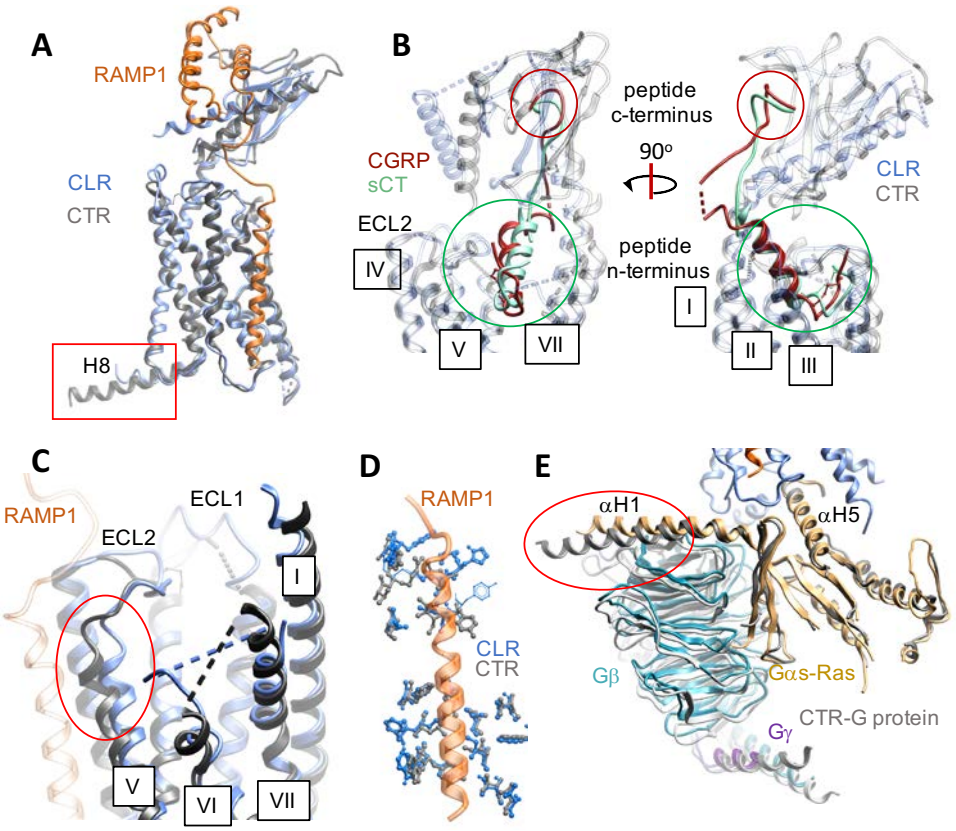
A
RAMP1
CLR
CTR
H8
B
CGRP
sCT
ECL2
IV
V
VII
peptide
c-terminus
90°
peptide
n-terminus
I
II
III
CLR
CTR
C
RAMP1
ECL1
ECL2
I
V
VI
VII
D
RAMP1
CLR
CTR
E
αH1
αH5
Gβ
Gαs-Ras
Gγ
CTR-G protein

Native protein sequence
HA signal peptide
FLAG epitope
3C cleavage site
His tag
TMs
Omitted residues due to lack of EM density
Stubbed residues

CLR – Expression construct

```
  1 MEKKCTLYFL VLLPFFMILV T
  1 MKTIIALSYI FCLVFADYKD DDDLEVLFQG PAELEESPED SIQLGVTRNK

 51 IMTAQYECYQ KIMQDPIQQA EGVYCNRTWD GWLCWNDVAA GTESMQLCPD

101 YFQDFDPSEK VTKICDQDGN WFRHPASNRT WTNYTQCNVN THEKVKTALN
                 stalk, TM1                          TM2
151 LFYLTIIGHG LSIASLLISL GIFFYFKSLS CQRITLHKNL FFSFVCNSVV
                                      TM3
201 TIIHLTAVAN NQALVATNPV SCKVSQFIHL YLMGCNYFWM LCEGIYLHTL
                          TM4
251 IVVAVFAEKQ HLMWYYFLGW GFPLIPACIH AIARSLYYND NCWISSDTHL
                 TM5                                    TM6
301 LYIIHGPICA ALLVNLFFLL NIVRVLITKL KVTHQAESNL YMKAVRATLI
                                   TM7
351 LVPLLGIEFV LIPWRPEGKI AEEVYDYIMH ILMHFQGLLV STIFCFFNGE
      H8
401 VQAILRRNWN QYKIQFGNSF SNSEALRSAS YTVSTISDGP GYSHDCPSEH

451 LNGKSIHDIE NVLLKPENLY NPAGLEVLFQ GPHHHHHHHH
```

RAMP1- Expression construct

```
  1 MARALCRLPR RGLWLLLAHH LFMTTA
  1 MKTIIALSYI FCLVFADYKD DDDKHGSCQE ANYGALLREL CLTQFQVDME
 51 AVGETLWCDW GRTIRSYREL ADCTWHMAEK LGCFWPNAEV DRFFLAVHGR
101 YFRSCPISGR AVRDPPGSIL YPFIVVPITV TLLVTALVVW QSKRTEGIV
```

CGRP

ACDTATCVTH RLAGLLSRSG GVVKNNFVPT NVGSKAF-NH_2

Extended Data Figure 1

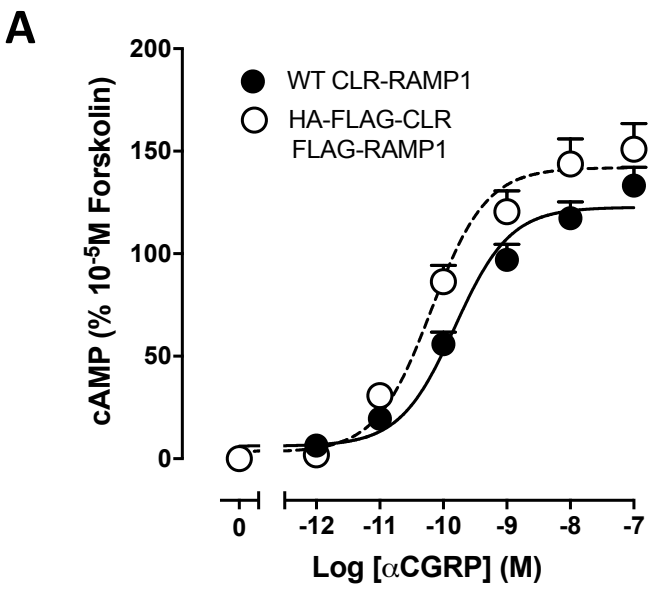

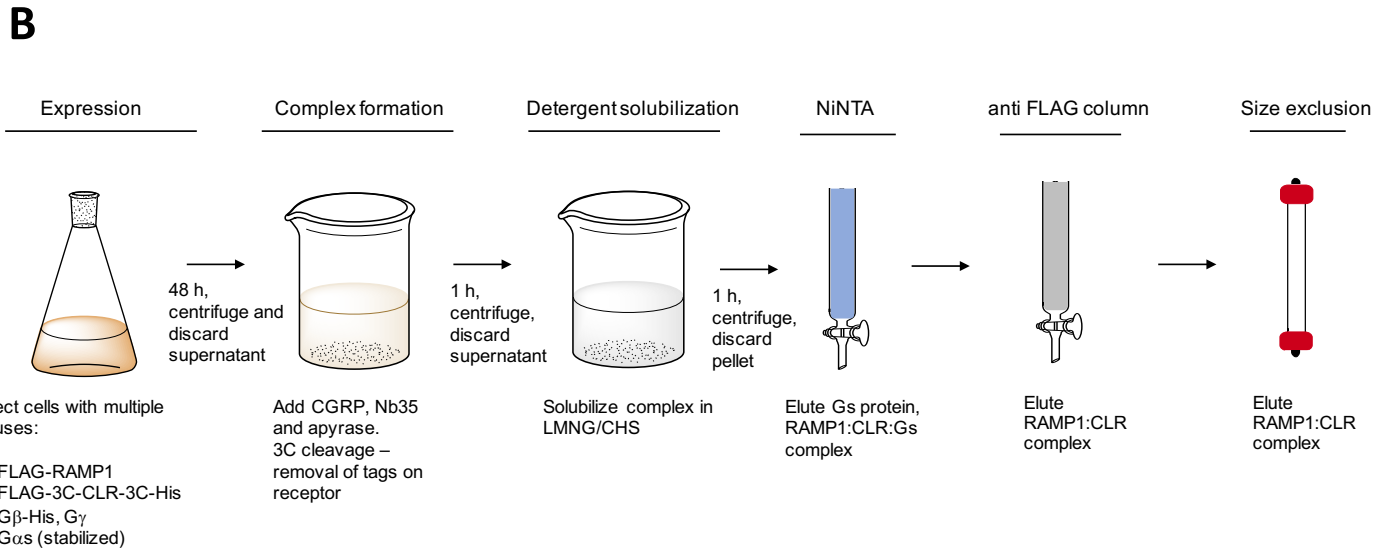

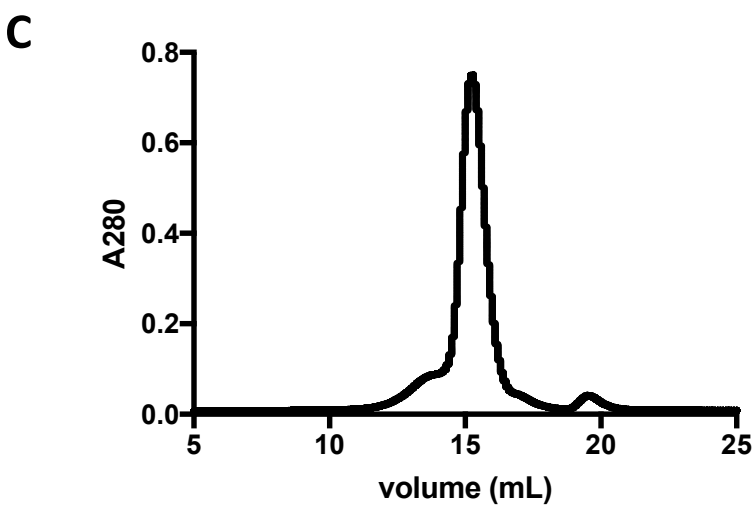

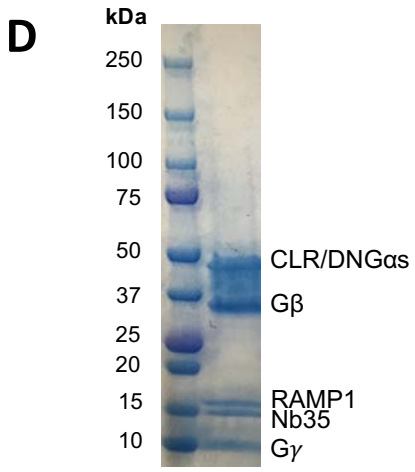

Extended Data Figure 2

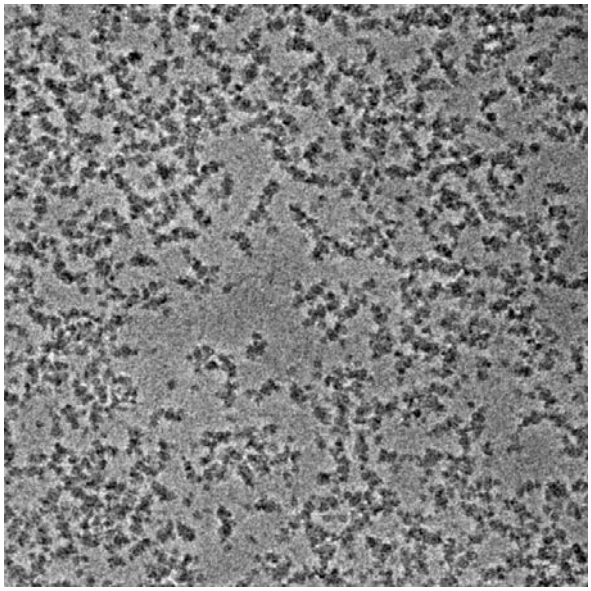

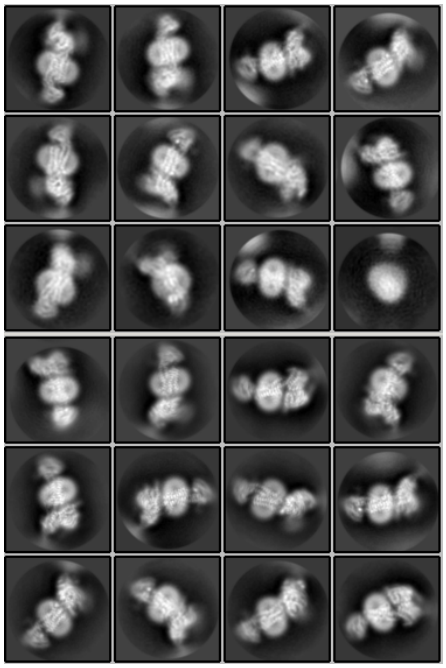

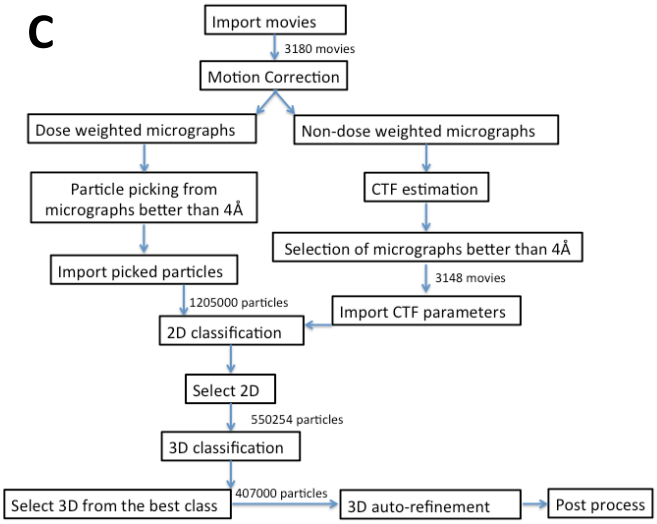

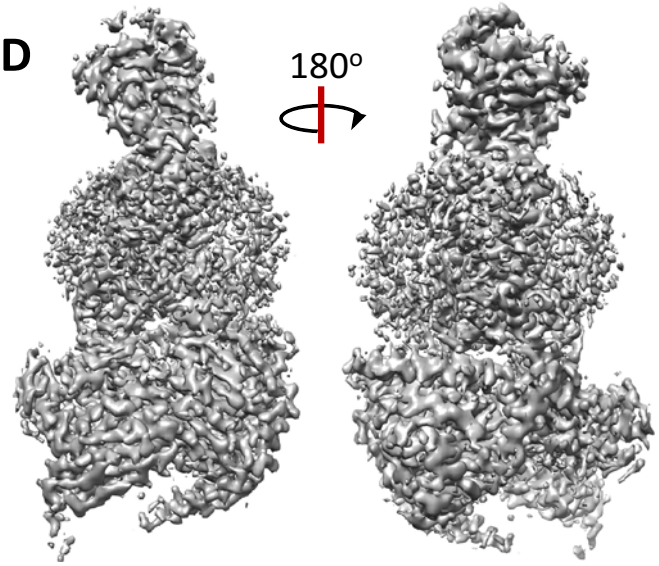

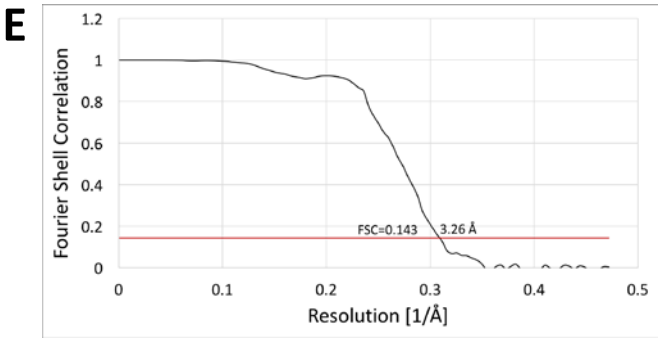

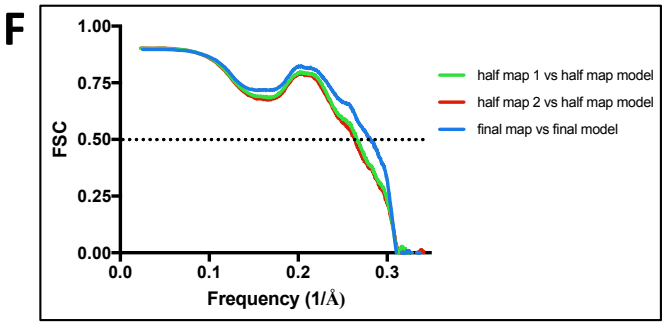

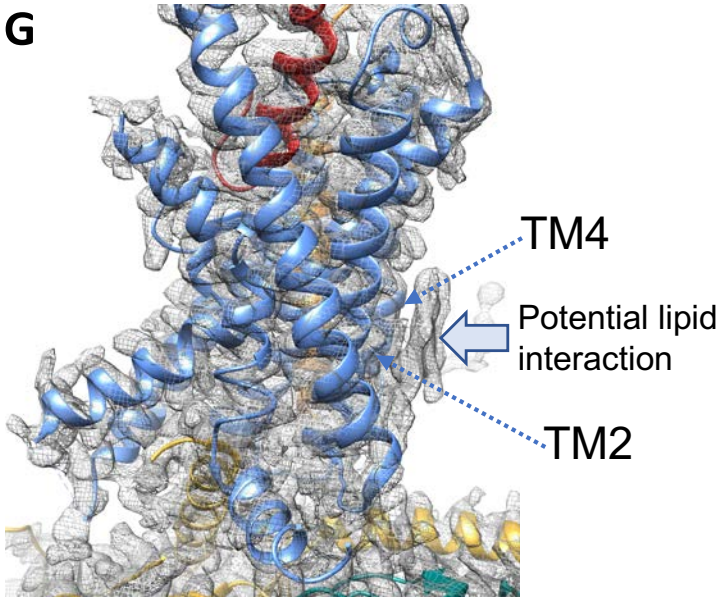

Extended Data Figure 3

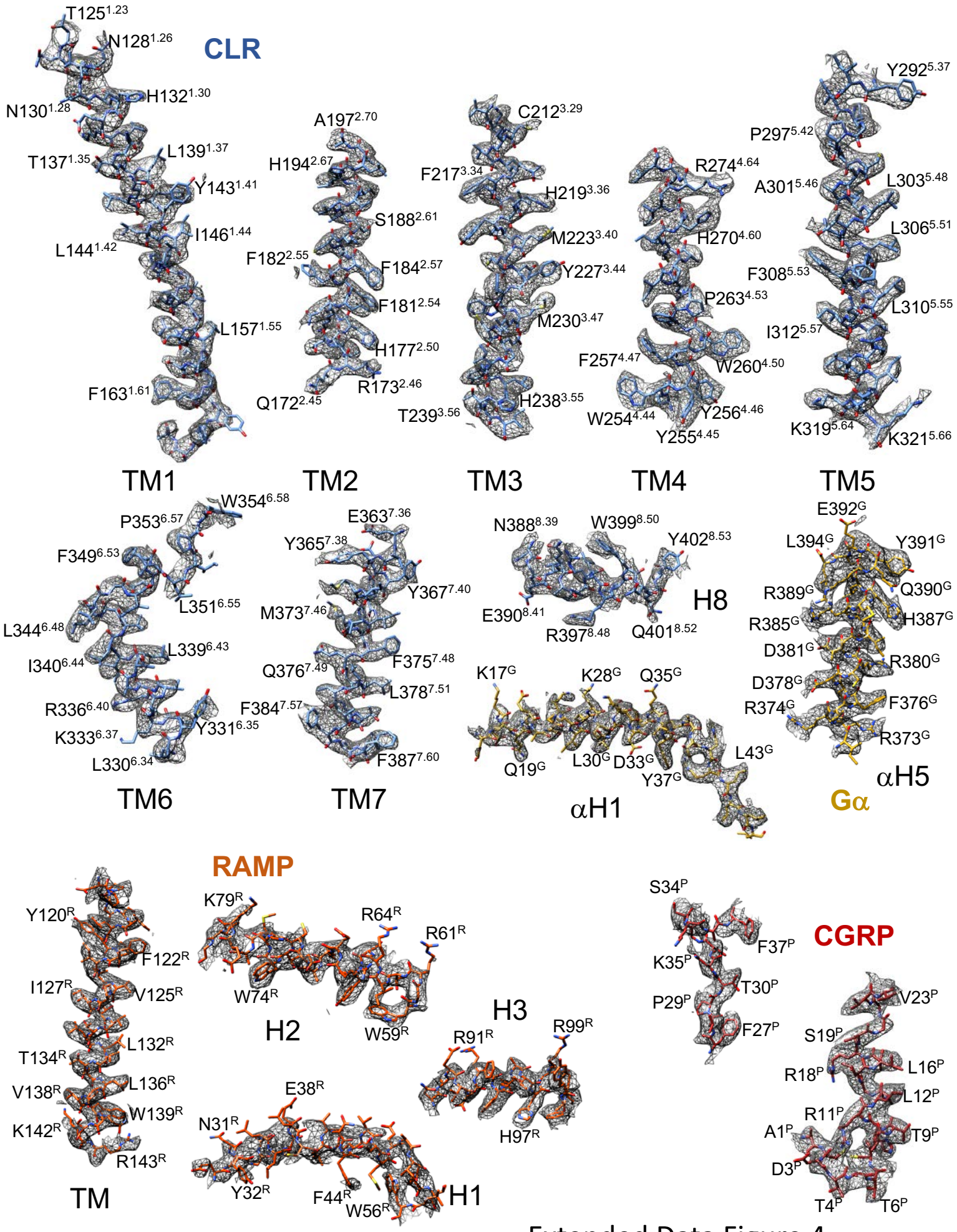

Extended Data Figure 4

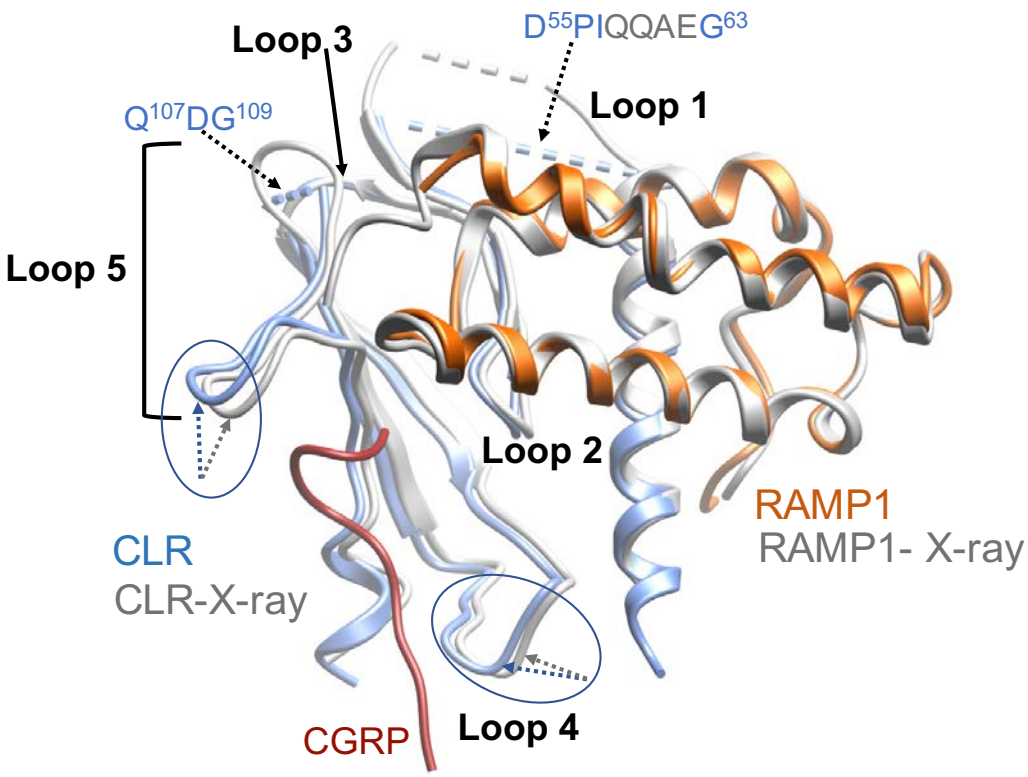

Extended Data Figure 5

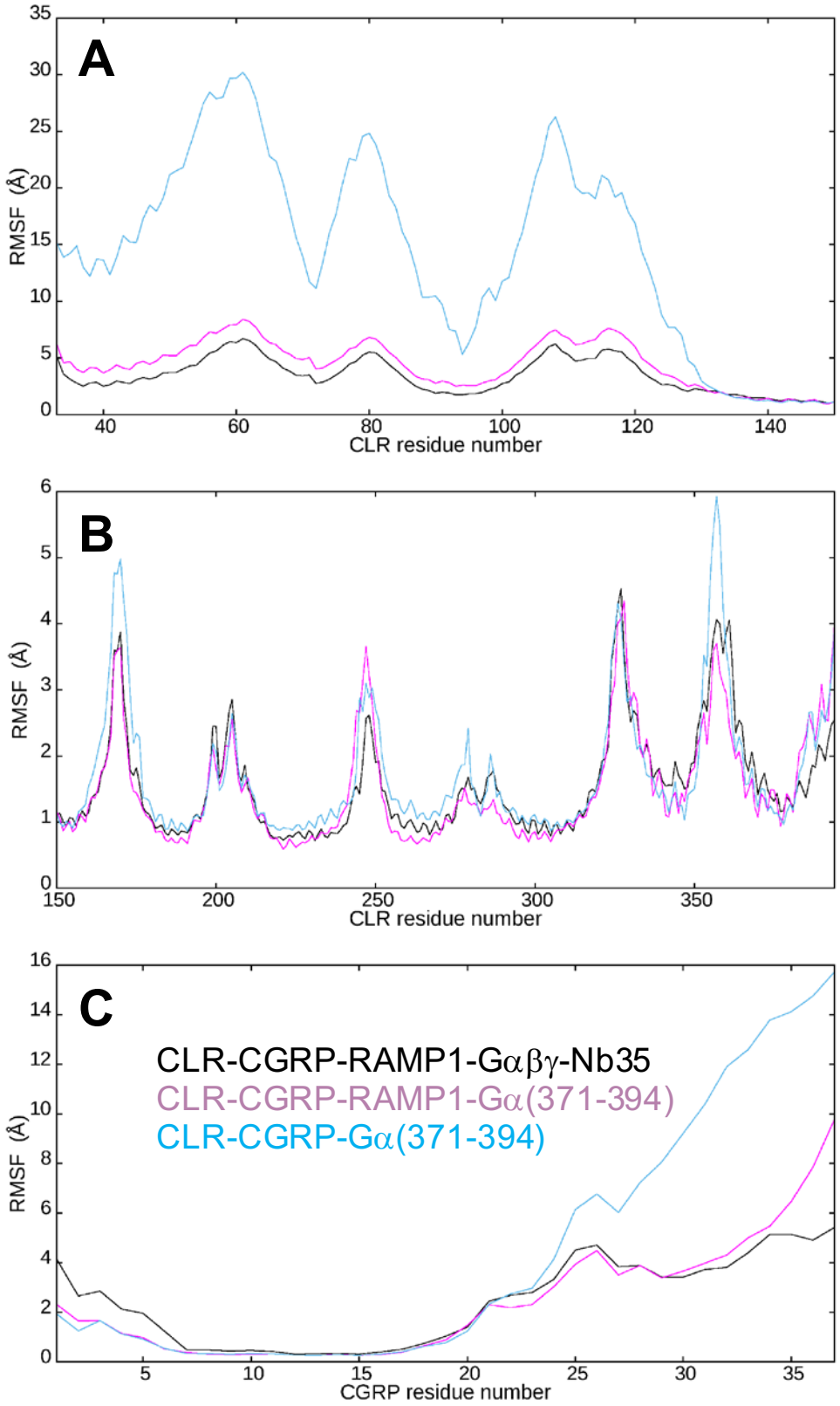

Extended Data Figure 6

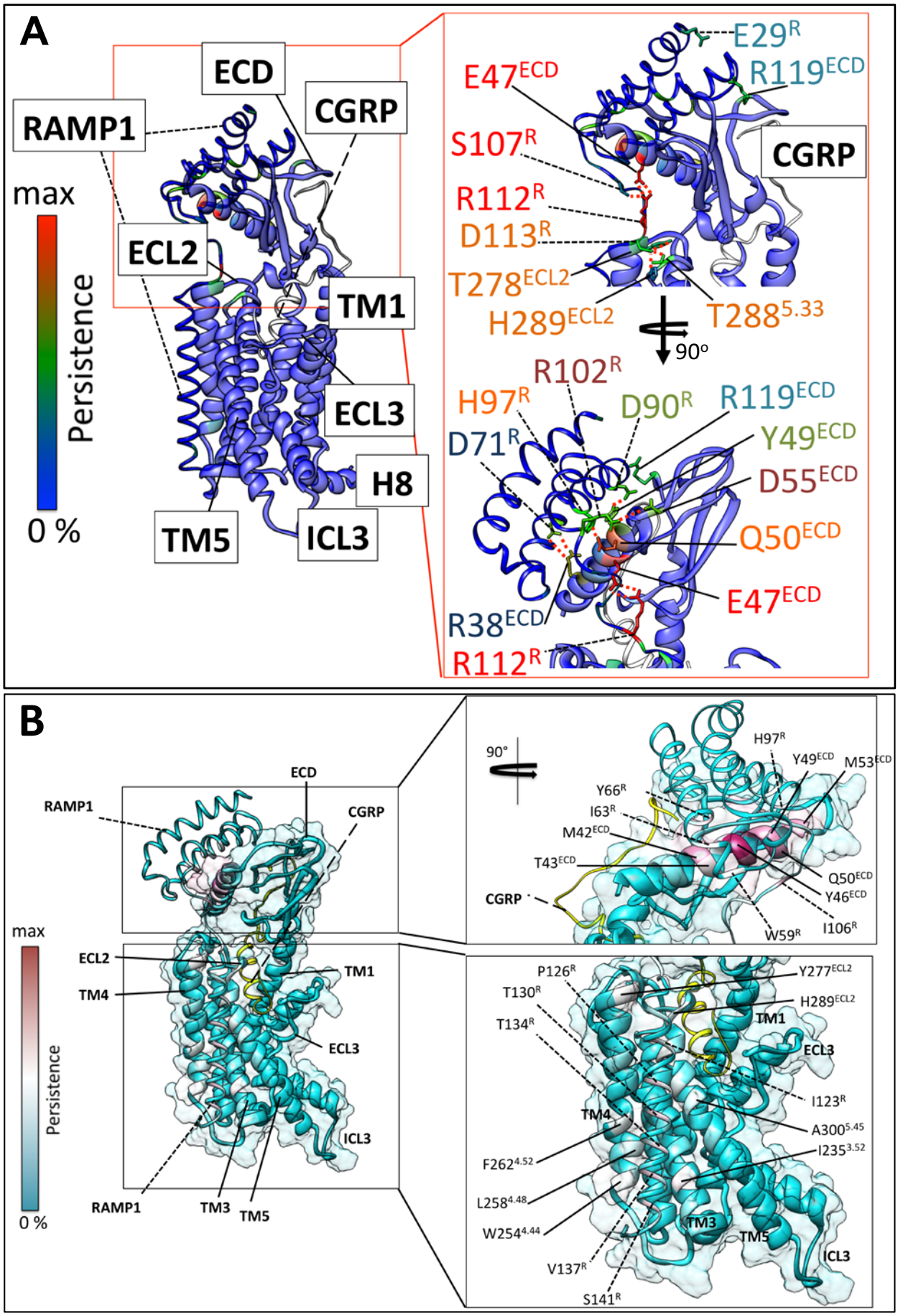

Extended Data Figure 7

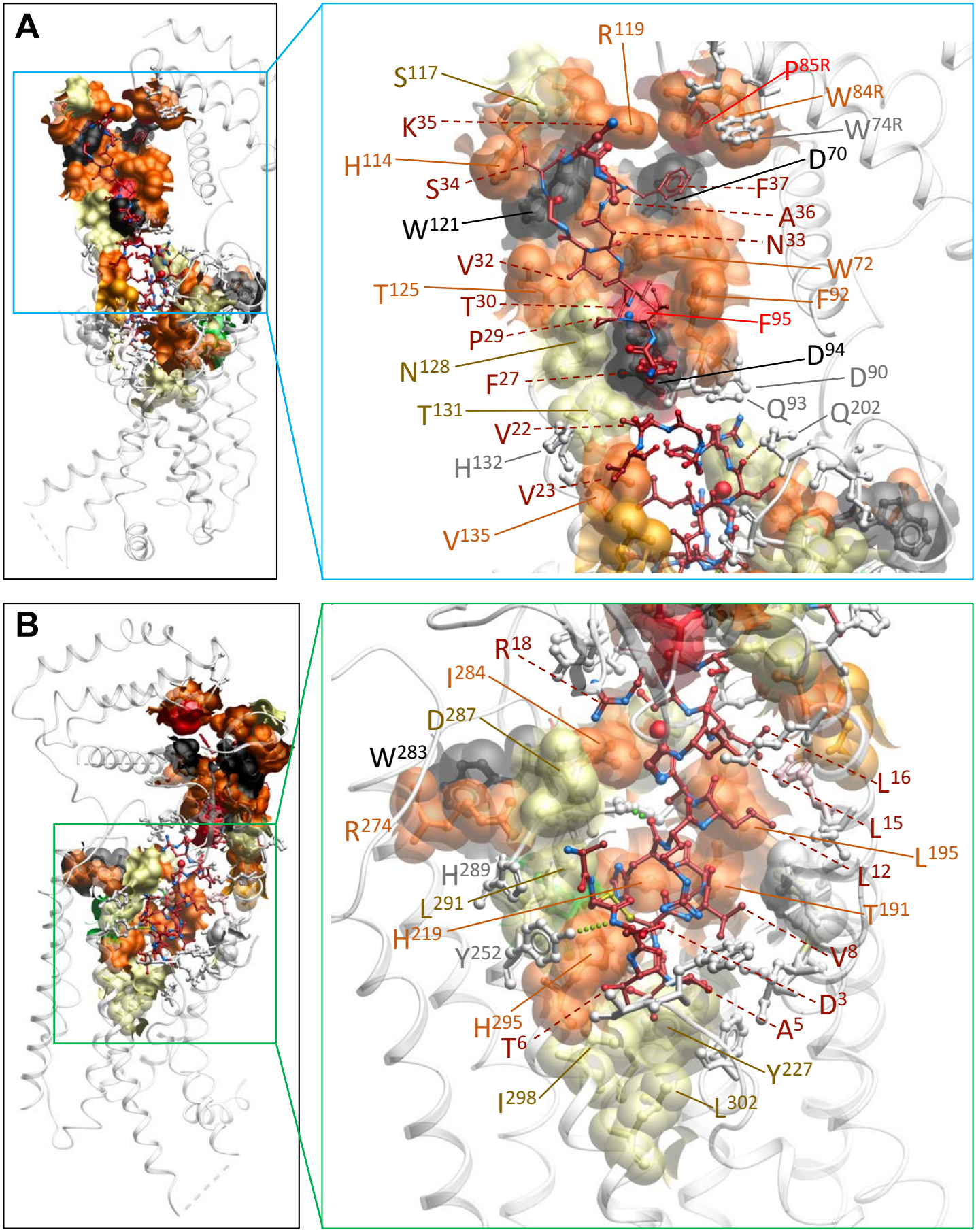

Extended Data Figure 8

Extended Data Figure 9

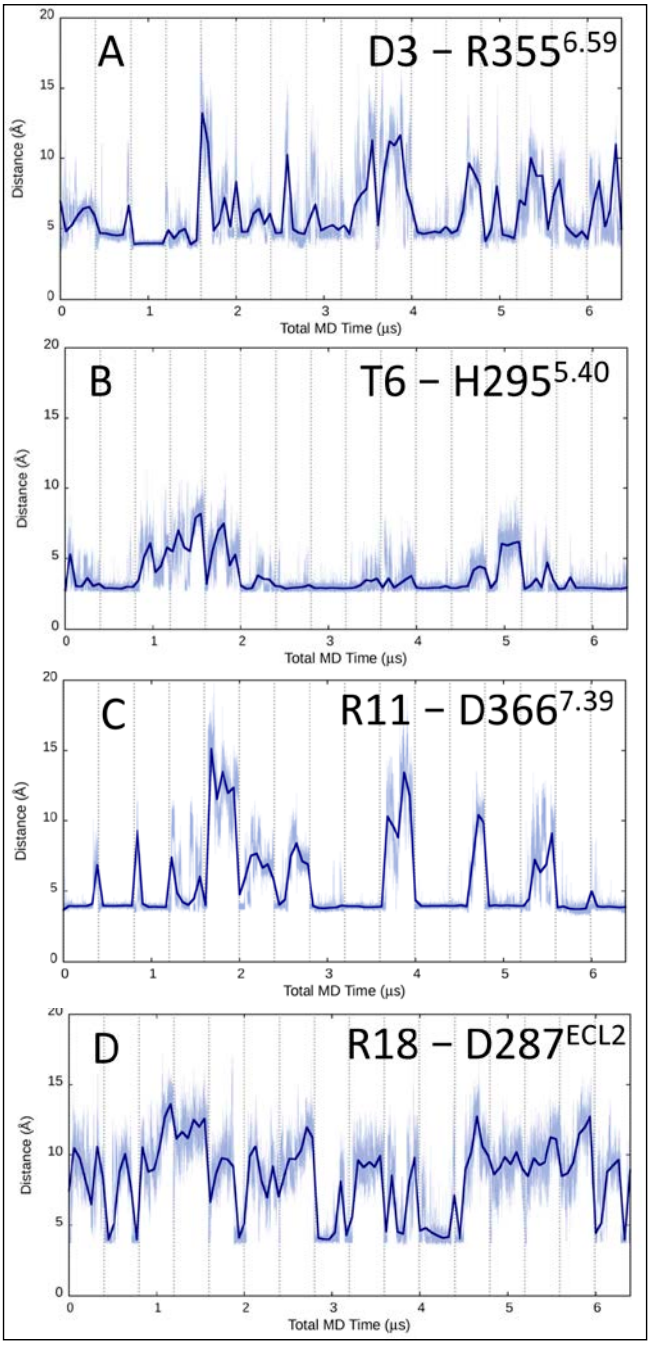

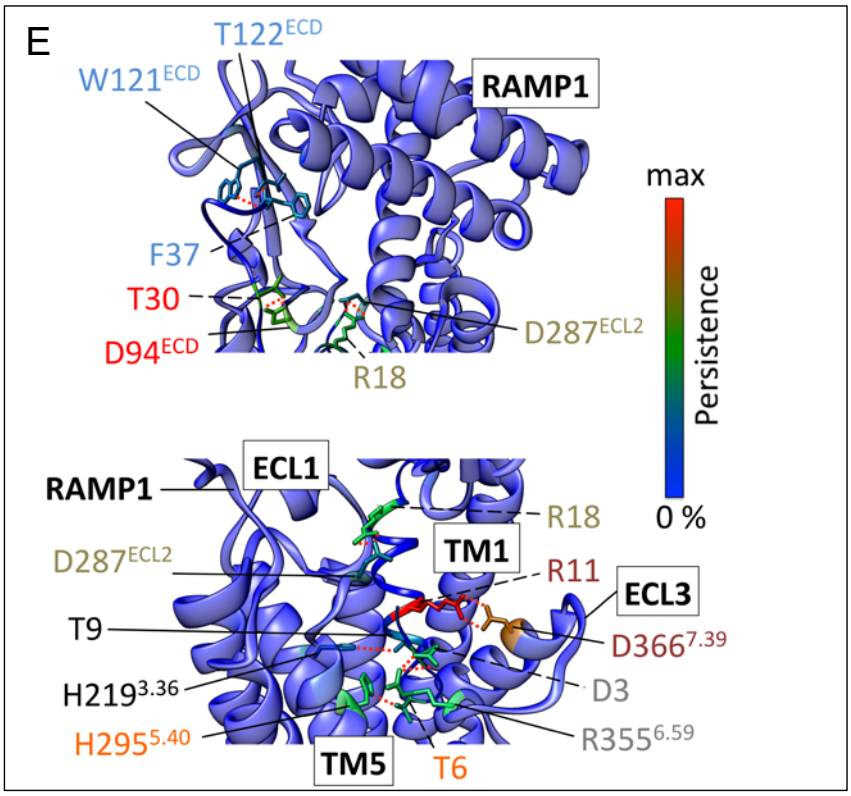

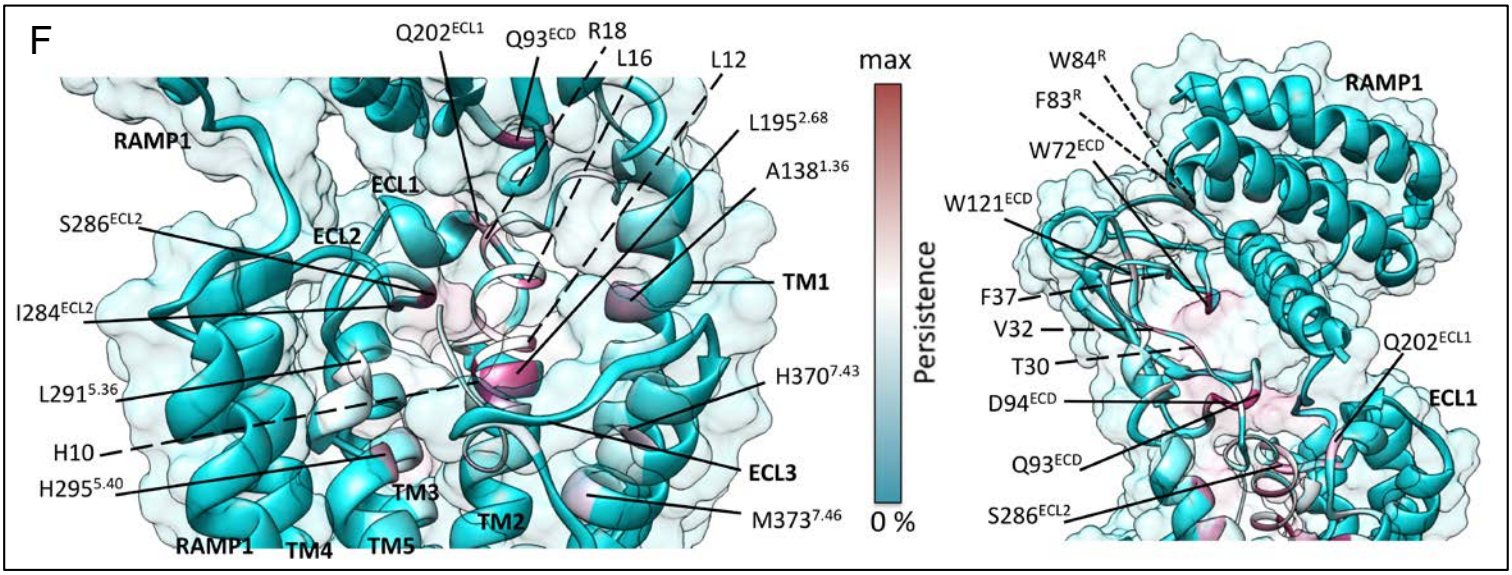

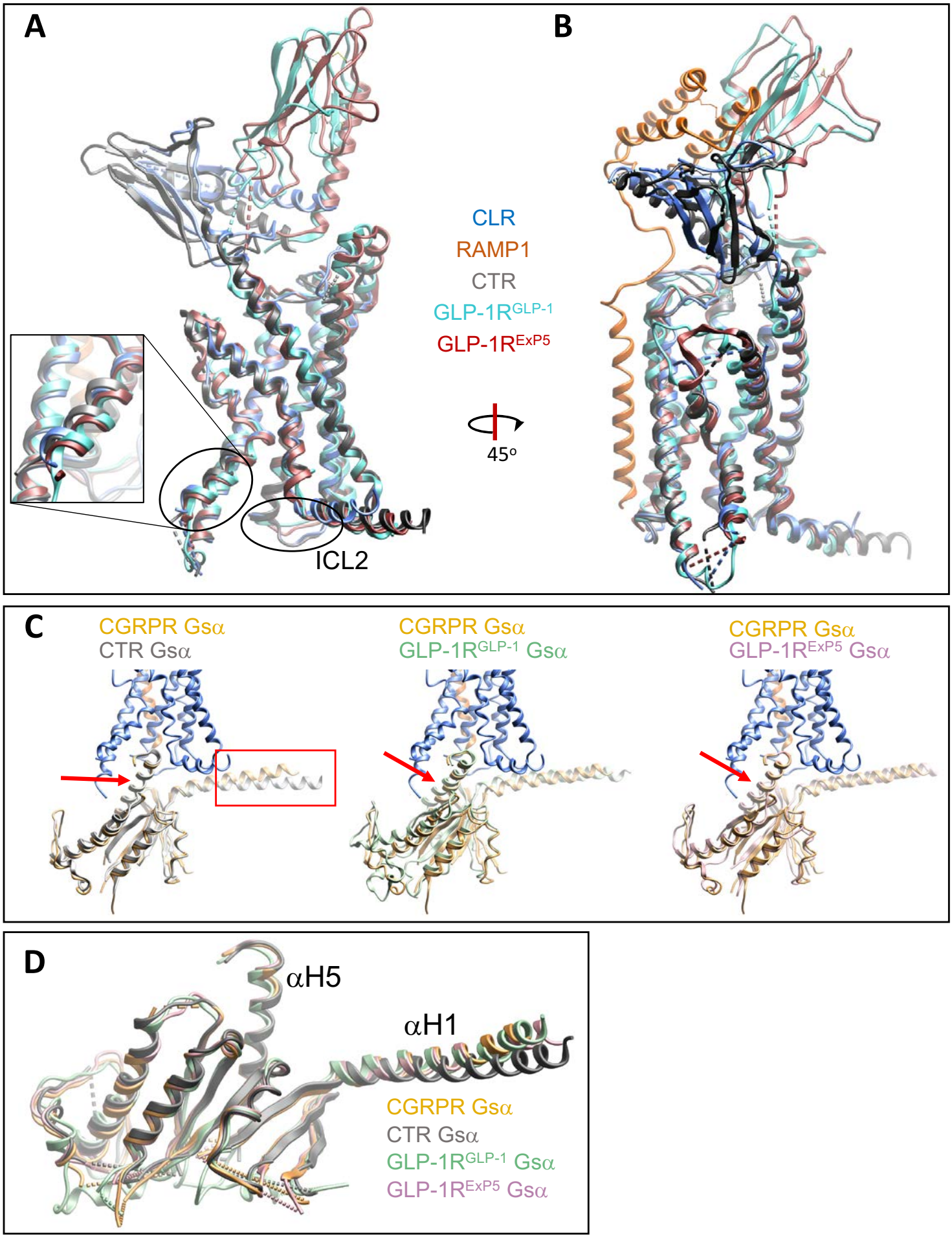

Extended Data Figure 10

Cryo-EM structure of the active, Gs-protein complexed, human CGRP receptor

Yi-Lynn Liang, Maryam Khoshouei, Giuseppe Deganuti, Alisa Glukhova, Cassandra Koole, Thomas S. Peat, Mazdak Radjainia, Jürgen M. Plitzko, Wolfgang Baumeister, Laurence J. Miller, Deborah L. Hay, Arthur Christopoulos, Christopher A Reynolds, Denise Wootten, Patrick M. Sexton

SUPPORTING INFORMATION

Supporting Information Table 1. A, PDB validation report. **B**, Cryo-EM data collection, refinement and validation statistics.

Supporting Information Table 2. Persistence of H-bonds and other contacts between RAMP1 and CLR in MD simulations.

Supporting Information Table 3. Persistence of H-bonds and other contacts between CGRP and CLR or RAMP1 in MD simulations.

Supporting Information Table 4. The difference in hydrogen bond formation between CGRP and CLR, during MD simulations performed on the CGRP-CLR-Gα(371-394) complex in the presence and absence of RAMP1.

Supporting Information Table 5. The difference in CLR intra-molecular hydrogen bonds formation in the presence or absence of RAMP1.

Supporting Information Table 6. Summary of all the MD simulations performed on the CLR-CGRP-RAMP1-G-protein.

Supporting Information Movie 1.
The CGRP (grey), CLR (green), RAMP1 (orange), G-protein (α subunit in blue, β subunit in red and γ subunit in yellow), Nb35 (maroon) complex simulated during a 400 ns long MD replica. Water molecules, ions and the lipid bilayer have been removed for clarity.

Supporting Information Movie 2.
Details of the extracellular TMs bundle during a 500 ns long MD replica, performed on the CGRP-CLR-RAMP1-G-protein complex. The hydrogen bonds formed between CGRP (orange), and CLR (cyan), and between CGRP (orange) and RAMP1 (green) are highlighted as dotted lines throughout the simulation.

Supporting Information Movie 3.
Comparison between two different 500 ns long MD simulations performed on: Left, CGRP (orange), CLR (green ribbon and transparent surface), RAMP1 (magenta ribbon and transparent surface), G-protein (371-394) complex. Right, CGRP (orange), CLR (green ribbon and transparent surface), G-protein (371-394) complex.

Supporting Information Table 1. A, PDB validation report. **B**, Cryo-EM data collection, refinement and validation statistics.

A

Full wwPDB/EMDataBank EM Map/Model Validation Report (i)

Jul 17, 2018 – 10:41 AM EDT

PDB ID	:	6E3Y
EMDB ID:	:	EMD-8978
Title	:	Cryo-EM structure of the active, Gs-protein complexed, human CGRP receptor
Deposited on	:	2018-07-16
Resolution	:	3.30 Å(reported)

This is a Full wwPDB/EMDataBank EM Map/Model Validation Report.

This report is produced by the wwPDB biocuration pipeline after annotation of the structure.

We welcome your comments at *validation@mail.wwpdb.org*
A user guide is available at
https://www.wwpdb.org/validation/2017/EMValidationReportHelp
with specific help available everywhere you see the (i) symbol.

MolProbity	:	4.02b-467
Percentile statistics	:	20171227.v01 (using entries in the PDB archive December 27th 2017)
Ideal geometry (proteins)	:	Engh & Huber (2001)
Ideal geometry (DNA, RNA)	:	Parkinson et. al. (1996)
Validation Pipeline (wwPDB-VP)	:	rb-20031172

1 Overall quality at a glance (i)

The following experimental techniques were used to determine the structure:
ELECTRON MICROSCOPY

The reported resolution of this entry is 3.30 Å.

Percentile scores (ranging between 0-100) for global validation metrics of the entry are shown in the following graphic. The table shows the number of entries on which the scores are based.

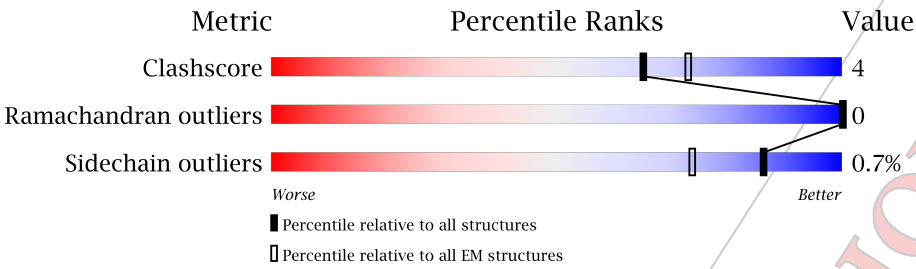

Metric	Whole archive (#Entries)	EM structures (#Entries)
Clashscore	136327	1886
Ramachandran outliers	132723	1663
Sidechain outliers	132532	1531

The table below summarises the geometric issues observed across the polymeric chains. The red, orange, yellow and green segments on the bar indicate the fraction of residues that contain outliers for >=3, 2, 1 and 0 types of geometric quality criteria. A grey segment represents the fraction of residues that are not modelled. The numeric value for each fraction is indicated below the corresponding segment, with a dot representing fractions <=5%

Mol	Chain	Length	Quality of chain
1	P	38	74% 18% 8%
2	N	138	81% 10% 9%
3	A	394	44% • • 52%
4	B	350	80% 16% •
5	G	71	65% • 31%
6	R	490	61% 9% 29%
7	E	149	68% 9% 23%

2 Entry composition (i)

There are 7 unique types of molecules in this entry. The entry contains 9434 atoms, of which 0 are hydrogens and 0 are deuteriums.

In the tables below, the AltConf column contains the number of residues with at least one atom in alternate conformation and the Trace column contains the number of residues modelled with at most 2 atoms.

- Molecule 1 is a protein called Calcitonin gene-related peptide 1.

Mol	Chain	Residues	Atoms					AltConf	Trace
			Total	C	N	O	S		
1	P	35	240	149	45	44	2	0	1

There is a discrepancy between the modelled and reference sequences:

Chain	Residue	Modelled	Actual	Comment	Reference
P	38	NH2	-	amidation	UNP P06881

- Molecule 2 is a protein called Nanobody 35.

Mol	Chain	Residues	Atoms					AltConf	Trace
			Total	C	N	O	S		
2	N	126	961	599	168	188	6	0	0

- Molecule 3 is a protein called Guanine nucleotide-binding protein G(s) subunit alpha isoforms short.

Mol	Chain	Residues	Atoms					AltConf	Trace
			Total	C	N	O	S		
3	A	188	1578	1009	290	274	5	0	0

There are 8 discrepancies between the modelled and reference sequences:

Chain	Residue	Modelled	Actual	Comment	Reference
A	54	ASN	SER	conflict	UNP P63092
A	226	ALA	GLY	conflict	UNP P63092
A	268	ALA	GLU	conflict	UNP P63092
A	271	LYS	ASN	conflict	UNP P63092
A	274	ASP	LYS	conflict	UNP P63092
A	280	LYS	ARG	conflict	UNP P63092
A	284	ASP	THR	conflict	UNP P63092
A	285	THR	ILE	conflict	UNP P63092

- Molecule 4 is a protein called Guanine nucleotide-binding protein G(I)/G(S)/G(T) subunit beta-1.

Mol	Chain	Residues	Atoms					AltConf	Trace
			Total	C	N	O	S		
4	B	336	2545	1573	455	496	21	0	0

There are 11 discrepancies between the modelled and reference sequences:

Chain	Residue	Modelled	Actual	Comment	Reference
B	-9	MET	-	initiating methionine	UNP P62873
B	-8	HIS	-	expression tag	UNP P62873
B	-7	HIS	-	expression tag	UNP P62873
B	-6	HIS	-	expression tag	UNP P62873
B	-5	HIS	-	expression tag	UNP P62873
B	-4	HIS	-	expression tag	UNP P62873
B	-3	HIS	-	expression tag	UNP P62873
B	-2	GLY	-	expression tag	UNP P62873
B	-1	SER	-	expression tag	UNP P62873
B	0	SER	-	expression tag	UNP P62873
B	1	GLY	-	expression tag	UNP P62873

- Molecule 5 is a protein called Guanine nucleotide-binding protein G(I)/G(S)/G(O) subunit gamma-2.

Mol	Chain	Residues	Atoms					AltConf	Trace
			Total	C	N	O	S		
5	G	49	372	234	63	72	3	0	0

- Molecule 6 is a protein called Calcitonin gene-related peptide type 1 receptor.

Mol	Chain	Residues	Atoms					AltConf	Trace
			Total	C	N	O	S		
6	R	346	2813	1859	459	471	24	0	0

There are 50 discrepancies between the modelled and reference sequences:

Chain	Residue	Modelled	Actual	Comment	Reference
R	-9	MET	-	initiating methionine	UNP Q16602
R	-8	LYS	-	expression tag	UNP Q16602
R	-7	THR	-	expression tag	UNP Q16602
R	-6	ILE	-	expression tag	UNP Q16602
R	-5	ILE	-	expression tag	UNP Q16602
R	-4	ALA	-	expression tag	UNP Q16602

Continued on next page...

Continued from previous page...

Chain	Residue	Modelled	Actual	Comment	Reference
R	-3	LEU	-	expression tag	UNP Q16602
R	-2	SER	-	expression tag	UNP Q16602
R	-1	TYR	-	expression tag	UNP Q16602
R	0	ILE	-	expression tag	UNP Q16602
R	1	PHE	-	expression tag	UNP Q16602
R	2	CYS	-	expression tag	UNP Q16602
R	3	LEU	-	expression tag	UNP Q16602
R	4	VAL	-	expression tag	UNP Q16602
R	5	PHE	-	expression tag	UNP Q16602
R	6	ALA	-	expression tag	UNP Q16602
R	7	ASP	-	expression tag	UNP Q16602
R	8	TYR	-	expression tag	UNP Q16602
R	9	LYS	-	expression tag	UNP Q16602
R	10	ASP	-	expression tag	UNP Q16602
R	11	ASP	-	expression tag	UNP Q16602
R	12	ASP	-	expression tag	UNP Q16602
R	13	ASP	-	expression tag	UNP Q16602
R	14	LEU	-	expression tag	UNP Q16602
R	15	GLU	-	expression tag	UNP Q16602
R	16	VAL	-	expression tag	UNP Q16602
R	17	LEU	-	expression tag	UNP Q16602
R	18	PHE	-	expression tag	UNP Q16602
R	19	GLN	-	expression tag	UNP Q16602
R	20	GLY	-	expression tag	UNP Q16602
R	21	PRO	-	expression tag	UNP Q16602
R	462	PRO	-	expression tag	UNP Q16602
R	463	ALA	-	expression tag	UNP Q16602
R	464	GLY	-	expression tag	UNP Q16602
R	465	LEU	-	expression tag	UNP Q16602
R	466	GLU	-	expression tag	UNP Q16602
R	467	VAL	-	expression tag	UNP Q16602
R	468	LEU	-	expression tag	UNP Q16602
R	469	PHE	-	expression tag	UNP Q16602
R	470	GLN	-	expression tag	UNP Q16602
R	471	GLY	-	expression tag	UNP Q16602
R	472	PRO	-	expression tag	UNP Q16602
R	473	HIS	-	expression tag	UNP Q16602
R	474	HIS	-	expression tag	UNP Q16602
R	475	HIS	-	expression tag	UNP Q16602
R	476	HIS	-	expression tag	UNP Q16602
R	477	HIS	-	expression tag	UNP Q16602
R	478	HIS	-	expression tag	UNP Q16602

Continued on next page...

Continued from previous page...

Chain	Residue	Modelled	Actual	Comment	Reference
R	479	HIS	-	expression tag	UNP Q16602
R	480	HIS	-	expression tag	UNP Q16602

- Molecule 7 is a protein called Receptor activity-modifying protein 1.

Mol	Chain	Residues	Atoms					AltConf	Trace
			Total	C	N	O	S		
7	E	115	925	600	158	160	7	0	0

There are 27 discrepancies between the modelled and reference sequences:

Chain	Residue	Modelled	Actual	Comment	Reference
E	0	MET	-	initiating methionine	UNP O60894
E	1	LYS	-	expression tag	UNP O60894
E	2	THR	-	expression tag	UNP O60894
E	3	ILE	-	expression tag	UNP O60894
E	4	ILE	-	expression tag	UNP O60894
E	5	ALA	-	expression tag	UNP O60894
E	6	LEU	-	expression tag	UNP O60894
E	7	SER	-	expression tag	UNP O60894
E	8	TYR	-	expression tag	UNP O60894
E	9	ILE	-	expression tag	UNP O60894
E	10	PHE	-	expression tag	UNP O60894
E	11	CYS	-	expression tag	UNP O60894
E	12	LEU	-	expression tag	UNP O60894
E	13	VAL	-	expression tag	UNP O60894
E	14	PHE	-	expression tag	UNP O60894
E	15	ALA	-	expression tag	UNP O60894
E	16	ASP	-	expression tag	UNP O60894
E	17	TYR	-	expression tag	UNP O60894
E	18	LYS	-	expression tag	UNP O60894
E	19	ASP	-	expression tag	UNP O60894
E	20	ASP	-	expression tag	UNP O60894
E	21	ASP	-	expression tag	UNP O60894
E	22	ASP	-	expression tag	UNP O60894
E	23	LYS	-	expression tag	UNP O60894
E	24	HIS	-	expression tag	UNP O60894
E	25	GLY	-	expression tag	UNP O60894
E	26	SER	-	expression tag	UNP O60894

3 Residue-property plots (i)

These plots are drawn for all protein, RNA and DNA chains in the entry. The first graphic for a chain summarises the proportions of the various outlier classes displayed in the second graphic. The second graphic shows the sequence view annotated by issues in geometry. Residues are color-coded according to the number of geometric quality criteria for which they contain at least one outlier: green = 0, yellow = 1, orange = 2 and red = 3 or more. Stretches of 2 or more consecutive residues without any outlier are shown as a green connector. Residues present in the sample, but not in the model, are shown in grey.

- Molecule 1: Calcitonin gene-related peptide 1

Chain P: 74% 18% 8%

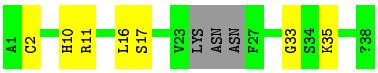

- Molecule 2: Nanobody 35

Chain N: 81% 10% 9%

- Molecule 3: Guanine nucleotide-binding protein G(s) subunit alpha isoforms short

Chain A: 44% • • 52%

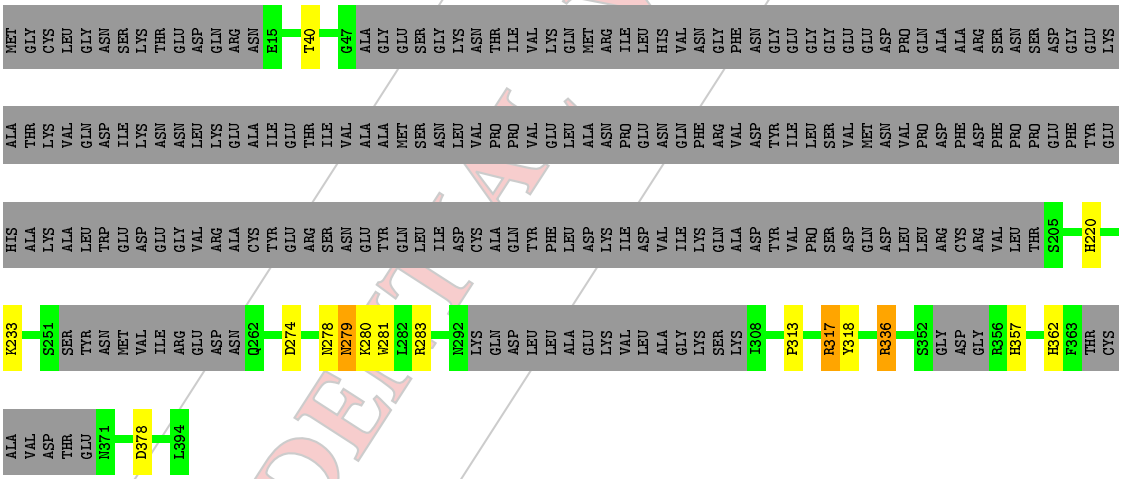

- Molecule 4: Guanine nucleotide-binding protein G(I)/G(S)/G(T) subunit beta-1

Chain B: 80% 16% •

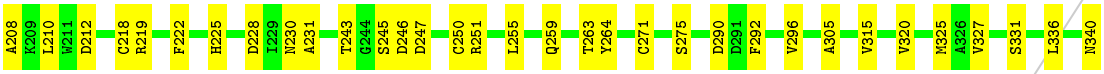

- Molecule 5: Guanine nucleotide-binding protein G(I)/G(S)/G(O) subunit gamma-2

Chain G:

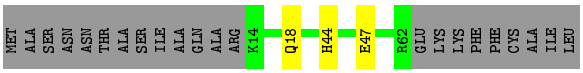

- Molecule 6: Calcitonin gene-related peptide type 1 receptor

Chain R:

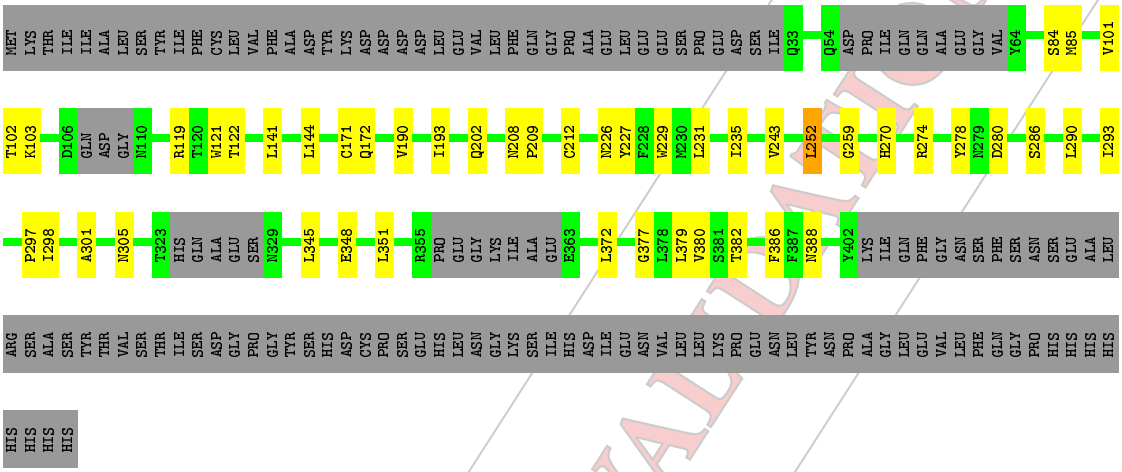

- Molecule 7: Receptor activity-modifying protein 1

Chain E:

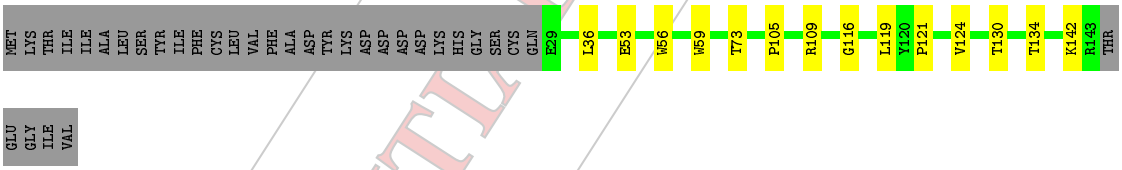

4 Experimental information (i)

Property	Value	Source
Reconstruction method	SINGLE PARTICLE	Depositor
Imposed symmetry	POINT, C1	Depositor
Number of particles used	407000	Depositor
Resolution determination method	FSC 0.143 CUT-OFF	Depositor
CTF correction method	NONE; phase plate CTF correction	Depositor
Microscope	FEI TITAN KRIOS	Depositor
Voltage (kV)	300	Depositor
Electron dose ($e^-/Å^2$)	50.0	Depositor
Minimum defocus (nm)	Not provided	Depositor
Maximum defocus (nm)	Not provided	Depositor
Magnification	47170	Depositor
Image detector	GATAN K2 SUMMIT (4k x 4k)	Depositor

5 Model quality (i)

5.1 Standard geometry (i)

Bond lengths and bond angles in the following residue types are not validated in this section: NH2

The Z score for a bond length (or angle) is the number of standard deviations the observed value is removed from the expected value. A bond length (or angle) with $|Z| > 5$ is considered an outlier worth inspection. RMSZ is the root-mean-square of all Z scores of the bond lengths (or angles).

Mol	Chain	Bond lengths		Bond angles	
		RMSZ	$\#\|Z\|>2$	RMSZ	$\#\|Z\|>2$
1	P	0.32	0/241	0.53	0/325
2	N	0.43	0/981	0.58	0/1329
3	A	0.38	0/1610	0.54	0/2162
4	B	0.43	0/2592	0.60	0/3519
5	G	0.31	0/378	0.51	0/513
6	R	0.38	0/2893	0.60	1/3942 (0.0%)
7	E	0.33	0/952	0.53	0/1299
All	All	0.39	0/9647	0.58	1/13089 (0.0%)

There are no bond length outliers.

All (1) bond angle outliers are listed below:

Mol	Chain	Res	Type	Atoms	Z	Observed(^{o})	Ideal(^{o})
6	R	252	LEU	CA-CB-CG	5.33	127.55	115.30

There are no chirality outliers.

There are no planarity outliers.

5.2 Too-close contacts (i)

In the following table, the Non-H and H(model) columns list the number of non-hydrogen atoms and hydrogen atoms in the chain respectively. The H(added) column lists the number of hydrogen atoms added and optimized by MolProbity. The Clashes column lists the number of clashes within the asymmetric unit, whereas Symm-Clashes lists symmetry related clashes.

Mol	Chain	Non-H	H(model)	H(added)	Clashes	Symm-Clashes
1	P	240	0	243	6	0
2	N	961	0	928	9	0
3	A	1578	0	1552	10	0

Continued on next page...

Continued from previous page...

Mol	Chain	Non-H	H(model)	H(added)	Clashes	Symm-Clashes
4	B	2545	0	2427	32	0
5	G	372	0	367	2	0
6	R	2813	0	2778	27	0
7	E	925	0	903	9	0
All	All	9434	0	9198	83	0

The all-atom clashscore is defined as the number of clashes found per 1000 atoms (including hydrogen atoms). The all-atom clashscore for this structure is 4.

All (83) close contacts within the same asymmetric unit are listed below, sorted by their clash magnitude.

Atom-1	Atom-2	Interatomic distance (Å)	Clash overlap (Å)
6:R:297:PRO:HB3	7:E:130:THR:HG21	1.74	0.68
4:B:71:VAL:HG22	4:B:81:ILE:HG12	1.77	0.65
3:A:313:PRO:O	3:A:317:ARG:NH1	2.32	0.63
6:R:172:GLN:HE21	6:R:252:LEU:HB2	1.65	0.61
4:B:95:LEU:HD13	4:B:100:VAL:HG21	1.83	0.61
1:P:33:GLY:O	6:R:121:TRP:NE1	2.33	0.61
2:N:29:PHE:O	2:N:72:ARG:NH2	2.34	0.60
1:P:17:SER:O	6:R:202:GLN:NE2	2.35	0.60
4:B:325:MET:O	4:B:340:ASN:ND2	2.36	0.59
3:A:362:HIS:NE2	3:A:378:ASP:OD2	2.35	0.59
4:B:315:VAL:HA	4:B:331:SER:HA	1.85	0.58
3:A:233:LYS:NZ	4:B:228:ASP:OD2	2.35	0.58
4:B:137:ARG:NE	4:B:171:ILE:O	2.36	0.58
4:B:271:CYS:HB2	4:B:290:ASP:HB3	1.85	0.58
6:R:379:LEU:HA	6:R:382:THR:HG22	1.86	0.57
6:R:243:VAL:HG11	7:E:142:LYS:HE2	1.88	0.55
4:B:230:ASN:ND2	4:B:246:ASP:OD1	2.38	0.55
2:N:52:SER:HB3	2:N:57:SER:HB3	1.89	0.55
2:N:52:SER:O	2:N:72:ARG:NH1	2.39	0.54
4:B:26:ALA:HB2	4:B:259:GLN:HE22	1.73	0.54
2:N:22:CYS:HB3	2:N:79:LEU:HB3	1.89	0.53
2:N:106:ASP:OD2	3:A:279:ASN:ND2	2.40	0.53
1:P:35:LYS:O	6:R:119:ARG:NH2	2.42	0.53
4:B:218:CYS:SG	5:G:18:GLN:NE2	2.81	0.52
4:B:51:LEU:HB2	4:B:336:LEU:HB2	1.91	0.52
6:R:270:HIS:HA	6:R:293:ILE:HD11	1.90	0.52
3:A:318:TYR:O	3:A:336:ARG:NH2	2.42	0.52
3:A:274:ASP:OD1	3:A:278:ASN:ND2	2.43	0.52
7:E:105:PRO:O	7:E:109:ARG:NH1	2.39	0.52

Continued on next page...

Continued from previous page...

Atom-1	Atom-2	Interatomic distance (Å)	Clash overlap (Å)
4:B:210:LEU:HD22	4:B:255:LEU:HD22	1.91	0.51
6:R:235:ILE:HD11	7:E:134:THR:HG23	1.92	0.51
7:E:59:TRP:HB2	7:E:109:ARG:HE	1.75	0.51
1:P:2:CYS:O	1:P:11:ARG:NH1	2.42	0.50
6:R:274:ARG:HE	6:R:290:LEU:HD23	1.76	0.50
4:B:145:TYR:O	4:B:162:GLY:N	2.45	0.50
6:R:209:PRO:HG2	6:R:212:CYS:HB2	1.94	0.49
6:R:85:MET:HA	6:R:101:VAL:O	2.12	0.49
4:B:212:ASP:OD2	4:B:219:ARG:NH2	2.45	0.49
1:P:10:HIS:O	6:R:286:SER:OG	2.30	0.49
6:R:231:LEU:HB2	6:R:301:ALA:HB1	1.94	0.49
6:R:171:CYS:SG	6:R:172:GLN:N	2.85	0.49
3:A:283:ARG:O	3:A:357:HIS:ND1	2.46	0.48
4:B:228:ASP:OD1	4:B:228:ASP:N	2.41	0.48
7:E:36:LEU:HD22	7:E:73:THR:HG22	1.96	0.48
5:G:44:HIS:ND1	5:G:47:GLU:OE2	2.38	0.48
7:E:116:GLY:HA2	7:E:119:LEU:HB3	1.96	0.47
6:R:227:TYR:HD2	6:R:298:ILE:HD13	1.80	0.47
6:R:382:THR:HA	6:R:386:PHE:HD2	1.79	0.47
2:N:63:SER:O	2:N:67:ARG:NH2	2.48	0.47
4:B:68:ARG:HH11	4:B:85:TYR:HD2	1.61	0.46
4:B:208:ALA:HB3	4:B:222:PHE:HB2	1.98	0.46
6:R:229:TRP:CE3	6:R:259:GLY:HA3	2.51	0.46
4:B:251:ARG:NH1	4:B:263:THR:OG1	2.49	0.45
4:B:165:THR:HG22	4:B:181:THR:HG22	1.97	0.45
4:B:58:ILE:HD13	4:B:336:LEU:HG	1.99	0.45
6:R:103:LYS:HB2	6:R:122:THR:HG23	1.99	0.45
2:N:15:GLY:HA2	2:N:85:SER:HA	1.99	0.44
4:B:296:VAL:O	4:B:305:ALA:N	2.49	0.44
2:N:102:PRO:HG2	4:B:247:ASP:HA	1.99	0.43
6:R:348:GLU:HG3	6:R:372:LEU:HD12	1.99	0.43
3:A:279:ASN:HD22	3:A:280:LYS:H	1.66	0.43
4:B:250:CYS:HB2	4:B:264:TYR:HB2	2.00	0.43
6:R:305:ASN:HB3	6:R:345:LEU:HB3	2.00	0.43
3:A:281:TRP:HH2	4:B:292:PHE:HE1	1.66	0.43
4:B:119:ASN:ND2	4:B:144:GLY:O	2.50	0.43
4:B:245:SER:OG	4:B:246:ASP:N	2.51	0.43
4:B:81:ILE:HD12	4:B:91:HIS:HB2	2.01	0.42
6:R:190:VAL:HA	6:R:193:ILE:HG12	2.00	0.42
6:R:278:TYR:CD2	6:R:280:ASP:HB2	2.54	0.42
1:P:16:LEU:HD23	1:P:16:LEU:HA	1.88	0.42

Continued on next page...

Continued from previous page...

Atom-1	Atom-2	Interatomic distance (Å)	Clash overlap (Å)
4:B:320:VAL:HG22	4:B:327:VAL:HG22	2.01	0.42
4:B:231:ALA:HB3	4:B:275:SER:HA	2.01	0.42
7:E:121:PRO:HA	7:E:124:VAL:HG22	2.01	0.42
2:N:9:GLY:HA2	2:N:124:VAL:HG22	2.02	0.41
6:R:141:LEU:HD23	6:R:144:LEU:HD21	2.02	0.41
6:R:377:GLY:HA2	6:R:380:VAL:HG12	2.02	0.41
6:R:348:GLU:HA	6:R:351:LEU:HB2	2.02	0.41
4:B:225:HIS:NE2	4:B:243:THR:OG1	2.36	0.41
6:R:84:SER:O	6:R:102:THR:HA	2.20	0.41
3:A:40:THR:HG23	3:A:220:HIS:HD2	1.84	0.41
4:B:59:TYR:HB2	4:B:75:GLN:HE21	1.86	0.41
4:B:79:LEU:HB3	4:B:93:ILE:HB	2.02	0.41
7:E:53:GLU:HA	7:E:56:TRP:CE2	2.56	0.41

There are no symmetry-related clashes.

5.3 Torsion angles (i)

5.3.1 Protein backbone (i)

In the following table, the Percentiles column shows the percent Ramachandran outliers of the chain as a percentile score with respect to all PDB entries followed by that with respect to all EM entries.

The Analysed column shows the number of residues for which the backbone conformation was analysed, and the total number of residues.

Mol	Chain	Analysed	Favoured	Allowed	Outliers	Percentiles	
1	P	31/38 (82%)	29 (94%)	2 (6%)	0	100	100
2	N	124/138 (90%)	120 (97%)	4 (3%)	0	100	100
3	A	176/394 (45%)	176 (100%)	0	0	100	100
4	B	334/350 (95%)	317 (95%)	17 (5%)	0	100	100
5	G	47/71 (66%)	47 (100%)	0	0	100	100
6	R	336/490 (69%)	329 (98%)	7 (2%)	0	100	100
7	E	113/149 (76%)	113 (100%)	0	0	100	100
All	All	1161/1630 (71%)	1131 (97%)	30 (3%)	0	100	100

There are no Ramachandran outliers to report.

5.3.2 Protein sidechains (i)

In the following table, the Percentiles column shows the percent sidechain outliers of the chain as a percentile score with respect to all PDB entries followed by that with respect to all EM entries.

The Analysed column shows the number of residues for which the sidechain conformation was analysed, and the total number of residues.

Mol	Chain	Analysed	Rotameric	Outliers	Percentiles	
1	P	26/29 (90%)	26 (100%)	0	100	100
2	N	104/115 (90%)	104 (100%)	0	100	100
3	A	166/349 (48%)	163 (98%)	3 (2%)	62	81
4	B	270/291 (93%)	269 (100%)	1 (0%)	92	95
5	G	39/58 (67%)	39 (100%)	0	100	100
6	R	306/437 (70%)	303 (99%)	3 (1%)	78	87
7	E	98/129 (76%)	98 (100%)	0	100	100
All	All	1009/1408 (72%)	1002 (99%)	7 (1%)	86	91

All (7) residues with a non-rotameric sidechain are listed below:

Mol	Chain	Res	Type
3	A	279	ASN
3	A	317	ARG
3	A	336	ARG
4	B	155	ASN
6	R	208	ASN
6	R	226	ASN
6	R	388	ASN

Some sidechains can be flipped to improve hydrogen bonding and reduce clashes. All (13) such sidechains are listed below:

Mol	Chain	Res	Type
1	P	10	HIS
3	A	23	ASN
3	A	278	ASN
3	A	279	ASN
4	B	88	ASN
4	B	155	ASN
4	B	259	GLN
4	B	268	ASN

Continued on next page...

Continued from previous page...

Mol	Chain	Res	Type
5	G	18	GLN
6	R	50	GLN
6	R	54	GLN
6	R	172	GLN
6	R	388	ASN

5.3.3 RNA (i)

There are no RNA molecules in this entry.

5.4 Non-standard residues in protein, DNA, RNA chains (i)

There are no non-standard protein/DNA/RNA residues in this entry.

5.5 Carbohydrates (i)

There are no carbohydrates in this entry.

5.6 Ligand geometry (i)

There are no ligands in this entry.

5.7 Other polymers (i)

There are no such residues in this entry.

5.8 Polymer linkage issues (i)

There are no chain breaks in this entry.

B

Cryo-EM data collection, refinement and validation statistics

	#1 name (EMDB EMD-8978) (PDB 6E3Y)
Data collection and processing	
Magnification	47170
Voltage (kV)	300
Electron exposure (e–/Å^2)	50
Defocus range (μm)	-0.6
Pixel size (Å)	1.06
Symmetry imposed	C1
Initial particle images (no.)	1,205,000
Final particle images (no.)	407,000
Map resolution (Å)	3.26
FSC threshold	0.143
Map resolution range (Å)	3.0-3.8
Refinement	
Initial model used (PDB code)	5UZ7, 4RWG, 6B3J
Model resolution (Å)	
FSC threshold	0.143
Model resolution range (Å)	3.26
Map sharpening *B* factor (Å^2)	-50
Model composition	
Non-hydrogen atoms	
Protein residues	1195
Ligands	
B factors (Å^2)	93-229 (avr. 148)
Protein	
Ligand	
R.m.s. deviations	
Bond lengths (Å)	0.007
Bond angles (°)	0.999
Validation	
MolProbity score	1.34
Clashscore	4.51
Poor rotamers (%)	0
Ramachandran plot	
Favored (%)	97.41
Allowed (%)	2.59
Disallowed (%)	0

Supporting Information Table 2. Hydrogen bonds and contacts formed between RAMP1 and CLR during molecular dynamics simulations. Persistence is defined as following: (total number of hydrogen bonds between two given residues / total number of frames) * 100; a persistence > 100% is possible when more than one hydrogen bond is observed between the two residues in a given frame. Hydrogen bonds with persistence > **1%** and contacts with persistence **> 20%** are shown. If not specified, a side chain-side chain hydrogen bond is reported, otherwise **bb**=backbone-backbone hydrogen bond; **sb**=side chain-backbone; **bs**=backbone-side chain; **tb**=terminus-backbone. Interactions to ECL2 ($Y277^{4.67}$-$H289^{5.66}$) and ECL3 ($G346^{6.50}$-$V364^{7.37}$) of CLR are shown in green and blue, respectively; interactions to the CLR ECD ($E29^{ECD}$-$T131^{ECD}$) are shown in grey. Interactions for the alternative RAMP1 C-terminus conformation are shown in *italics* for residues $S141^{R}$ – $V148^{R}$. CLR residues involved in hydrogen bonds with persistence grater than 25 are shown in **bold;** CLR residues involved in multiple hydrogen bonds to a given RAMP1 residue and for which the sum of the persistence is greater than 25 are shown in bold and are underlined. CLR residues involved in contacts with persistence greater than 50 are shown in **bold** and are **<u>underlined</u>**.

RAMP1 residue	CLR hydrogen bonds (% frames)	CLR contacts (% frames)
Glu29	<u>Arg119 34.56</u>	**Arg119 27.3**
Cys57	/	**Tyr46 35.8**
Trp59	**Thr43 16.66** **Asn39 1.90**	Thr43 100.0 Tyr46 99.5 Met42 96.2
Ile63	/	Asn39 98.2 Met42 90.0 Thr43 68.5
Tyr66	**Gln45 6.57**	Gln45 100.0 Met42 99.8 Tyr46 99.3 Tyr49 89.3
Arg67	/	Met42 99.8 Arg38 95.0 **Asn39 26.2**
Ala70	/	Met42 95.5 Gln45 77.2 **Arg38 27.3**
Asp71	<u>Arg38 75.84</u>	**Arg38 78.6**
Phe83	/	Arg119 91.9 **Ser117 34.5**
Trp84	**Arg119 2.38 (bs)**	**Met 42 21.4** **Arg119 20.7**
Pro85	**Arg119 2.39 (bs)**	Gly71 78.8 Asp70 69.8 **Arg119 27.1** **Trp69 27.1**
Asn86	/	**Arg119 31.5**
Asp90	Tyr49 64.91	Tyr49 100.0 **Thr68 20.2**
Phe93	/	Tyr49 99.2 Gln45 89.5

Leu94	/	Ile52 99.8 Met53 99.4 Tyr49 93.1
His97	Gln50 55.75	Gln50 100.0 Tyr49 100.0 Tyr46 100.0 Met53 95.8
Gly98	/	Met53 91.1
Phe101	/	Gln50 100.0 Tyr46 99.3 Met53 58.7
Arg102	Asp55 65.81 **Gln54 1.04**	Met53 92.7 Asp55 64.5 **Gln54 31.3**
Cys104	/	Gln50 99.8 Tyr46 69.6
Pro105	**Tyr46 15.19 (bs)** **Gln50 10.49 (bs)**	Gln50 99.6
Ile106	/	**Tyr46 41.3**
Ser107	Glu47 25.19	Glu47 94.9 **Lys51 35.8**
Gly108	**Glu47 23.90 (bs)**	Glu47 87.9
Arg109	/	Thr43 88.3 Tyr46 75.3 Glu47 67.8
Ala110	**Glu47 24.24 (bs)**	Thr43 90.0 Glu47 67.6
Val111	/	Tyr278 89.5 **Tyr277 40.2** **Lys40 22.7**
Arg112	Glu47 101.94 **Asp90 10.80**	Glu47 83.4 Tyr278 72.0 **Tyr277 41.8**
Asp113	Thr288 49.20 **His289 33.99 (sb)** Tyr278 32.81 **His289 18.00**	His289 86.3 Tyr278 73.6 Thr288 72.3 **Leu290 47.7** **Tyr277 21.7**
Pro114	/	Tyr277 91.1 Leu290 85.1 **Tyr278 35.4**
Ile118	/	**Tyr277 53.0**
Leu119	/	His289 93.6 Leu290 80.1 **Ile293 28.4**
Phe122	/	Ile293 94.7 Ile269 82.7 Ala273 71.7 Tyr277 54.1 **Leu290 35.5** **Leu276 23.4** **Ile272 22.3**

Ile123	/	Tyr292 99.6 Ile293 92.1 His289 55.5
Pro126	/	Pro297 98.5 Ile293 96.8 Pro266 83.6 Ile269 68.5
Ile127	/	Gly296 98.4 Pro297 97.1 Ala300 95.7
Val129	/	Phe262 97.5
Thr130	/	Phe262 99.8 Pro297 99.6 Phe228 97.6 Ala300 72.2 **Ala301 30.5**
Leu131	/	Ala300 78.0 Val304 66.4
Val133	/	Leu258 99.0 Phe262 90.1 Phe257 67.9
Thr134	/	Leu231 98.9 Ile235 98.8 Val302 95.6 Leu258 68.5
Leu136	/	Trp254 67.9
Val137	/	Trp254 99.4 Leu258 98.3 Ile235 95.6 Tyr255 88.8 **Phe257 26.5**
Val138	/	Ile235 99.2 Phe308 86.1 **His238 22.5**
Gln140	/	Trp254 98.0 **His251 22.2**
Ser141	**Tyr255 22.72** **Thr239 6.24** ***Thr239 12.37 (bs)*** ***Tyr255 8.55*** ***Thr239 6.54*** ***Gln250 6.19 (bs)*** ***Tyr255 2.97***	Thr239 91.2 Tyr255 86.6 Ile235 75.1 Gln250 54.9 **His251 29.4** *Tyr255 95.5* *Thr239 92.3* *Ile235 84.5* *Gln250 69.0*
Lys142	**Glu248 1.47**	Val243 92.1 Thr239 66.0 Ala244 50.5 *Val243 89.8*

		Ala244 78.8 *Thr239 72.4*
Arg143	**Gln250 1.15 (bs)** ***Gln250 1.41 (bs)***	***/*** ***Gln250 34.7*** ***His251 20.4***
Thr144	**Lys249 2.35 (sb)** ***Lys249 1.67 (bs)***	**Lys249 35.2** **Ala247 34.7** **Phe246 22.0** **Gln250 21.1** ***Ala247 49.3*** ***Phe246 42.2*** ***Gln250 39.5*** ***Ala244 35.5*** ***Lys249 28.1***
Glu145	**Lys 249 4.61** ***Lys249 3.76*** ***Lys249 3.66 (bb)***	**Lys249 23.7** **His251 20.2** ***Gln250 41.4*** ***Lys249 39.0*** ***His251 35.8***
Gly146	**Trp254 2.24 (bs)** ***His251 1.62 (sb)***	**Lys249 22.4** ***His251 24.2***
Ile147	***/*** ***/***	**His251 26.3** ***His251 20.9***
Val148	**Lys249 3.75** **His251 2.89 (sb)** ***Lys249 2.19***	**His251 24.5**

Supporting Information Table 3. Hydrogen bonds and contacts formed between CGRP and CLR/RAMP1 during molecular dynamics simulations. Persistence is defined as the (total number of hydrogen bonds between two given residues / total number of frames) * 100; a persistence > 100% is possible when more than one hydrogen bond is observed between the two residues in a given frame. Hydrogen bonds with persistence > **1%** and contacts with persistence **> 20%** are shown. If not specified, a side chain-side chain hydrogen bond is reported, otherwise **bb**=backbone-backbone hydrogen bond; **sb**=side chain-backbone; **bs**=backbone-side chain; **tb**=terminus-backbone. Interactions to ECL1 (T196$^{2.69}$-P209$^{3.74}$), ECL2 (Y277$^{4.67}$-H289$^{5.66}$) and ECL3 (G346$^{6.50}$-V364$^{7.37}$) of CLR are shown in red, green and blue respectively; interactions to the CLR ECD (Q33^{ECD}-T131^{ECD}) are shown in grey. CLR residues involved in multiple hydrogen bonds to a given CGRP residue and for which the sum of the persistence is greater than 25 are shown in **bold** and are **<u>underlined</u>**.

CGRP residue	CLR hydrogen bonds (% frames)	CLR contacts (% frames)	RAMP1 hydrogen bonds (% frames)	RAMP1 contacts (% frames)
A1	**Asp287 3.76 (bs)** **His289 3.71 (bs)** **Asp366 2.59 (bs)**	Asp287 52.4 **Ser286 37.1** **Tyr292 34.7** **His289 27.8** **Arg355 27.5**	/	/
C2	**Arg355 1.29 (bs)**	Ser286 65.7 Leu291 63.4 **Tyr292 47.1** **His295 24.2**	/	/
D3	<u>Arg355 34.71</u> **Tyr292 7.50** **Lys359 3.78**	Arg355 79.0 Trp354 62.4 **Tyr292 42.5**	/	/
T4	**His295 1.19**	His295 74.0 **Trp354 47.8** **Cys299 35.0** **Tyr292 26.8**	/	/
A5	/	Phe349 84.5 Met373 62.6 Met369 57.4 **Trp354 42.2** **Tyr227 21.9**	/	/
T6	His295 31.13	His295 81.5 Ile298 74.6 Tyr227 70.5 Met223 68.8 **Met373 38.2** **Phe349 35.9** **Leu302 27.0**	/	/
C7	/	His295 60.3 Leu291 60.3 **Ser286 45.6**	/	/
V8	/	His370 96.4 Met373 95.9	/	/

		Met369 71.0 **His374 33.7** **Trp354 24.6**		
T9	**His219 18.98** **His374 2.16**	Thr191 92.7 Leu195 87.0 His219 76.9 His194 59.6 Met373 52.7 His374 51.6 **Met223 37.2**	/	/
H10	**His295 7.46** **Arg274 2.48**	Ser286 91.1 Ile284 69.8 Leu220 69.3 Leu291 69.2 Gln216 69.1 His219 62.9 **His295 44.7** **His194 43.3** **Trp283 26.2** **Met223 23.9** **Ser285 21.7**	/	/
R11	Asp366 85.37 **Asp96 8.37** **Asp287 6.24**	Ser286 73.6 Asp366 71.3 His370 61.6 **Trp354 25.1**	/	/
L12	/	Leu141 97.4 Leu195 95.4 Thr145 85.3 His370 83.6 Phe142 65.9 His374 61.3 **Ala138 43.0**	/	/
A13	/	Leu195 95.2 Ile284 90.8 His194 71.9 Ala199 54.5 **Val198 49.9**	/	/
G14	/	**Ile284 77.0** **Ser286 22.5**	/	/
L15	/	**Ala138 99.2** **Lys134 67.3** **Leu141 48.5**	/	/
L16	/	Phe142 99.6 Ala199 98.2 Leu195 90.3 Ala138 74.1 Leu139 58.1 **Val198 38.9** **Asn200 36.7**	/	/
S17	**Gln202 2.95 (bs)**	Ile284 68.2 Gln202 63.4 Ala199 59.4	/	/

		Val198 47.5 **Leu204 32.0** **Val205 28.8**		
R18	**Asp287 22.96** **Asp90 4.47** **Asp96 4.31**	Pro97 92.2 Gln93 87.6 Phe95 52.5 Asp96 51.7 **Asp90 34.8** **Asp287 23.9**	/	/
S19	**Gln93 7.74 (sb)**	Val135 99.5 Ala138 75.9 **Leu139 28.1**	/	/
G20	/	**Gln202 68.7**	/	/
G21	/	Gln93 78.2 Gln202 53.8	/	/
V22	/	Val135 91.3 Asp94 90.1 Gln93 87.5 Thr131 79.3 **His132 36.8**	/	/
V23	/	Val135 83.8 Leu139 60.0	/	/
K24	**Gln202 1.45**	Gln202 65.2	/	/
N25	/	/	/	/
N26	/	/	/	/
F27	/	Asp94 90.8 Gln93 73.7	/	/
V28	/	/	/	/
P29	/	Asp94 89.2 **Asn128 21.6**	/	/
T30	Asp94 62.32 Asp94 56.01 **(bs)**	Asp94 96.7 Asn128 93.4 Phe95 93.2 Phe92 92.9 Trp72 75.6	/	/
N31	/	Trp72 77.6	/	/
V32	/	Tyr124 93.2 Phe95 92.2 Thr125 90.5 Asn128 88.1 Trp72 67.1 Trp121 50.6	/	/
G33	**Trp121 17.80 (bs)**	Trp121 55.9	/	/
S34	**Arg119 6.20 (bs)** **Ser117 3.66 (bs)** **His114 3.33**	Trp121 51.4 **His114 49.7** **Arg119 43.0** **Ser117 40.1** **Ala116 21.1**	**Trp84 1.36**	**Phe83 26.5**
K35	**Arg119 1.07 (bs)**	**Arg119 34.4**	**Glu78 7.77**	Phe83 55.5
A36	**R119 6.04 (bs)**	Trp72 54.6	/	/

		Trp121 50.2 **Arg119 28.6**		
F37	**T122 11.48 (tb)** **T122 8.22 (bb)** **Asp70 1.62**	Trp72 89.4 Gly71 79.2 Tyr124 55.6 Asp70 52.7 **Thr122 34.5** **Trp121 30.1** **Arg119 22.8**	/	Trp84 87.9 Pro85 78.9 Trp74 57.7 **Phe83 22.4**

Supporting Information Table 4. The difference in hydrogen bond formation between CGRP and CLR, during MD simulations performed on the CGRP-CLR-Gα (371-394) complex in the presence and absence of RAMP1. Hydrogen bond persistence is expressed as percentage on the total duration of the simulations (2.0 μs for each system). Hydrogen bonds with persistence > **5%** are shown: **sb**=side chain-backbone; **bs**=backbone-side chain; **ts**=terminus-side chain. If not specified, a side chain-side chain hydrogen bond is reported. A persistence > 100% is possible when more than one hydrogen bond is possible between the two residues. The persistence of hydrogen bonds involving Asp^{3}, Thr^{6}, Thr^{9}, His^{10} (and Phe^{37}) are unchanged upon loss of RAMP1, consistent with the low RMSFs in this region. The main loss of interactions is in the C-terminus; this is consistent with the higher RMSF for this region. Moreover, this may affect the proposed two-stage binding mechanism for class B peptide ligands[S1] in which the initial binding involves the C-terminus.

CGRP residue	Hydrogen bond persistence (% frames)				Variation
	With RAMP1		Without RAMP1		
Ala^{1}	H289^{ECL2}	17.4 (ts)	H289^{ECL2}	10.0	↓
Arg^{11}	D366^{ECL3}	108.6	D366^{ECL3}	134.0	↑↑
Arg^{18}	D287^{ECL2}	72.9	D287^{ECL2}	45.1	↓↓↓
	D90^{ECD}	14.9	/		↓
Ser^{19}	Q93^{ECD}	7.1 (sb)	/		↓
Thr^{30}	D94^{ECD}	61.1	D94^{ECD}	31.0	↓↓↓
	D94^{ECD}	54.7 (bs)	D94^{ECD}	27.5 (bs)	↓↓↓

Persistence change: ↑↑= 15-30% increase; ↓= 5-15% decrease; ↓↓= 15-30%; ↓↓↓= 30+% decrease. Details of the CLR – CGRP and RAMP1 – CLR interactions are available from the University of Essex Research Repository (doi to be provided).

Supporting Information Table 5. The difference in CLR intra-molecular hydrogen bonds formation in the presence or absence of RAMP1. Persistence during MD simulations performed on the CGRP-CLR-Gα(371-394) complex in the presence and absence of RAMP1. Hydrogen bond persistence is expressed as percentage on the total duration of the simulations (2.0 μs for each system). **sb**=side chain-backbone; **bs**=backbone-side chain. If not specified, a side chain-side hydrogen bond is reported. A persistence > 100% is possible when more than one hydrogen bonds are possible between the two residues.

CLR intra-molecular Hydrogen bond	Hydrogen bond persistence (% frames)		Variation
	With RAMP1	Without RAMP1	
R173$^{2.46}$ - E233$^{3.50}$	214.5	125.2	↓↓↓↓
R274$^{4.64}$ - D280^{ECL2}	157.4	5.8	↓↓↓↓↓
K134$^{1.32}$ - D96^{ECD}	70.4	38.0	↓↓↓
K134$^{1.32}$ - A138$^{1.36}$ (sb)	63.5	49.8	↓
K134$^{1.32}$ - N130$^{1.28}$ (sb)	36.7	29.9	↓
K134$^{1.32}$ - E99^{ECD}	32.9	9.7	↓↓
D67^{ECD} - D77^{ECD}	58.4	77.5	↑↑
D67^{ECD} - D77^{ECD} (bs)	46.9	32.1	↓
D67^{ECD} - K51^{ECD} (sb)	16.1	39.1	↑↑
D108^{ECD} - R113^{ECD}	37.6	79.2	↑↑↑

Persistence change: ↑↑= 15-30% increase; ↑↑↑= 30-50% increase; ↑↑↑↑= 50-100%% increase; ↓= 5-15% decrease; ↓↓= 15-30%; ↓↓↓= 30-50% decrease; ↓↓↓↓= 50-100% decrease; ↓↓↓↓↓=>100% decrease. Values over 100% arise through multiple hydrogen bonds.

Supporting Information Table 6. Summary of all the MD simulations performed on the CLR-CGRP-RAMP1-G-protein. CLR conformation #4 is the original PLOP-derived conformation; CLR conformations #0-3 were taken from the 4 highest occupied clusters. αβγ denotes the full G-protein, while α371-394 denotes the C terminal helix αH5 (N371 - L394) of the G-protein α subunit.

Conformation		G protein	Number of replicas	Total MD sampling time
ECL3	RAMP1 C-term			
#0	#1	αβγ	4	1.6 μs
#1	#1	αβγ	4	1.6 μs
#2	#1	αβγ	4	1.6 μs
#3	#1	αβγ	4	1.6 μs
#1	#2	αβγ	10	2.4 μs
Total CLR:CGRP:RAMP1:αβγ simulation time				***8.8 μs***
#4	#1	($\alpha_{371-394}$)	4	2.0 μs
#4	N/A	($\alpha_{371-394}$)	4	2.0 μs

Supporting Information specific references

S1. de Graaf, C., *et al.,* Extending the structural view of class B GPCRs. *Trends Biochem Sci* **42**, 946−960 (2017).